STRESS ANALYSIS OF A HELICAL GEAR TRANSMISSION PICKUP CAR USING MECHANICAL TESTS AND FINITE ELEMENT METHOD

A THESIS

BY

VISANU BOONMAG

Presented in Partial Fulfillment of the Requirements for the

Master of Engineering Degree in Mechanical Engineering

at Srinakharinwirot University

June 2016

การวิเคราะห์ความเค้นที่ส่งผ่านเฟืองเฉียงรถยนต์บรรทุกขนาดเล็ก
โดยใช้การทดสอบทางกลและวิธีไฟไนต์เอลิเมนต์

ปริญญานิพนธ์

ของ

วิษณุ บุญมาก

เสนอต่อบัณฑิตวิทยาลัย มหาวิทยาลัยศรีนครินทรวิโรฒ เพื่อเป็นส่วนหนึ่งของการศึกษา
ตามหลักสูตรปริญญาวิศวกรรมศาสตรมหาบัณฑิต สาขาวิชาวิศวกรรมเครื่องกล
มิถุนายน 2559

การวิเคราะห์ความเค้นที่ส่งผ่านเฟืองเฉียงรถยนต์บรรทุกขนาดเล็ก
โดยใช้การทดสอบทางกลและวิธีไฟไนต์เอลิเมนต์

ปริญญานิพนธ์

ของ

วิษณุ บุญมาก

เสนอต่อบัณฑิตวิทยาลัย มหาวิทยาลัยศรีนครินทรวิโรฒ เพื่อเป็นส่วนหนึ่งของการศึกษา
ตามหลักสูตรปริญญาวิศวกรรมศาสตรมหาบัณฑิต สาขาวิชาวิศวกรรมเครื่องกล

มิถุนายน 2559

STRESS ANALYSIS OF A HELICAL GEAR TRANSMISSION PICKUP CAR USING
MECHANICAL TESTS AND FINITE ELEMENT METHOD

AN ABSTRACT

BY

VISANU BOONMAG

Presented in Partial Fulfillment of the Requirements for the
Master of Engineering Degree in Mechanical Engineering
at Srinakharinwirot University
June 2016

Visanu Boonmag. (2016). *Stress Analysis of a Helical Gear Transmission Pickup Car Using Mechanical Tests and Finite Element Method*, M.Eng (Mechanical Engineering). Bangkok: Graduate School, Srinakharinwirot University. Advisor Committee; Assoc. Prof. Dr. Ganwarich Pluphrach, Prof. Dr. Hadi Sutanto.

The fracture of a driving helical gear in the 5^{th} position gearing system in the gear-box of pick-up car which was to adjust the engine to increase horsepower. The helical gear was made from chromium steel JIS-SCr 420. It has been determined in many ways on the failure analysis of this helical gear i.e. 1) Composition (wt%) analysis with a spectrometer**,** 2) Vickers test, 3) Microstructural analysis with optical microscope, which the crack of the surface layer and energy dispersive spectroscopy using a scanning electron microscope, 4) Helical gear's AGMA bending stress and AGMA contact stress equation analysis and 5) All results compared with the finite element method. The analysis of summary results of this driving helical gear was determined with a fatigue fracture, which the load of contact stress over took the tensile strength of the material (1,300 MPa). The fracture characteristic of the helical gear's surface was expected with the fracture as transgranular and Intergranular, which had been absolutely observed as the brittle fracture. On the axial of helical gear was fractured as the cleavage features and pitting. This mixing failure area can be illustrated by the brittle and ductile fracture. It can be seen that the mixing failure area of oxide inclusion with carbide surrounding before the liquid state of material will be solidified which caused the failure of this driving helical gear. The summary analysis results can be accorded with the assumption of this research and as the information for a protection of any failure gearing.

Keywords: helical gear, failure, fatigue, Pick-up car

การวิเคราะห์ความเค้นที่ส่งผ่านเฟืองเฉียงรถยนต์บรรทุกขนาดเล็ก
โดยใช้การทดสอบทางกลและวิธีไฟไนต์เอลิเมนต์

บทคัดย่อ

ของ

วิษณุ บุญมาก

เสนอต่อบัณฑิตวิทยาลัย มหาวิทยาลัยศรีนครินทรวิโรฒ เพื่อเป็นส่วนหนึ่งของการศึกษา

ตามหลักสูตรปริญญาวิศวกรรมศาสตรมหาบัณฑิต สาขาวิชาวิศวกรรมเครื่องกล

มิถุนายน 2559

วิษณุ บุญมาก. (2559). *การวิเคราะห์ความเค้นที่ส่งผ่านเฟืองเฉียงรถยนต์บรรทุกขนาดเล็กโดยใช้การทดสอบทางกลและวิธีไฟไนต์เอลิเมนต์* ปริญญานิพนธ์ วศ.ม.(วิศวกรรมเครื่องกล). กรุงเทพฯ: บัณฑิตวิทยาลัย มหาวิทยาลัยศรีนครินทรวิโรฒ. คณะกรรมการควบคุม: รองศาสตราจารย์ ดร.กัณวริช พลูปราชญ์, ศาสตราจารย์ ดร.ฮาดี ซูตันโต

การแตกหักของเฟืองเฉียงขับที่ตำแหน่งเกียร์ 5 ในรถปิ๊กอัพคันหนึ่งซึ่งมีการปรับแต่งเครื่องยนต์ให้มีแรงม้าเพิ่มขึ้น เฟืองทำจากเหล็กกล้าผสมต่ำ JIS-SCr 420 การวิเคราะห์ความเสียหายของเฟืองมีหลายวิธีคือ 1) การวิเคราะห์ส่วนผสมทางเคมีด้วยเครื่อง Spectrometer 2) การตรวจสอบความแข็งด้วยวิธีวิกเกอร์ส 3) การวิเคราะห์โครงสร้างจุลภาคด้วยกล้องจุลทรรศน์แบบใช้แสง สำหรับการตรวจสอบโครงสร้างจุลภาคและการวิเคราะห์ธาตุเชิงปริมาณ พิจารณาด้วยกล้องจุลทรรศน์อิเล็กตรอนแบบส่องกราด 4) การวิเคราะห์ความเค้นดัดและความเค้นสัมผัสของเฟืองด้วยสมการ AGMA และ 5) การเปรียบเทียบผลลัพธ์ทั้งหมดร่วมกับวิธีไฟไนต์เอลิเมนต์ ผลของการวิเคราะห์สรุปได้ว่า การแตกหักของเฟืองเฉียงขับเกิดจากความล้าซึ่งเป็นผลมาจากความเค้นสัมผัสที่เกินค่า Tensile strength ของวัสดุ 1300 MPa ลักษณะรอยแตกบริเวณผิวรอบนอกของเฟืองมีการแตกผ่านเกรน (Transgranular) และการแตกระหว่างเกรน (Intergranular) ซึ่งเป็นการแตกหักแบบเปราะ ส่วนที่แกนกลางของเฟืองมีการแตกแบบแยกออก (Cleavage) และแบบรอยบุ๋ม (Dimples) ความเสียหายในบริเวณนี้เป็นแบบผสมมีการแตกหักแบบเปราะและแบบเหนียวปนกัน โดยที่สามารถเห็นการรวมเป็นส่วนผสมของออกไซด์ล้อมรอบด้วยคาร์ไบด์ (Oxide inclusion) ก่อนที่จะมีการเปลี่ยนสถานะจากของเหลวเป็นของแข็ง (Solidification) ซึ่งเป็นเหตุแห่งความเสียหายที่เกิดขึ้นในฟันเฟืองเฉียงขับดังกล่าว ทั้งนี้ผลของการวิเคราะห์สอดคล้องกับสมมติฐานที่ได้กำหนดไว้พร้อมเป็นข้อมูลสำหรับการหาวิธีป้องกันมิให้เกิดการชำรุดของเฟืองต่อไป

คำสำคัญ: เฟืองเฉียง, การแตกหัก, ความล้า, รถยนต์บรรทุกขนาดเล็ก

The thesis titled

"Stress Analysis of a Helical Gear Transmission Pickup Car Using

Mechanical Tests and Finite Element Method"

By

Visanu Boonmag

Has been approved by the Graduate School as partial fulfillment of the requirement for the Master of Engineering degree in Mechanical Engineering of Srinakharinwirot University

……………………………………………….. Acting Dean of Graduate School

(Assoc. Prof. Dr. Parin Chaivisuthangkura)

June……, 2016

Thesis Committee	Oral Defense Committee
…………………………….. Major-advisor	……………………………. Chair
(Assoc. Prof. Dr. Ganwarich Pluphrach)	(Asst. Prof. Dr. Siriporn Rojananan)
……………………………. Co-advisor	……………………………. Committee
(Prof. Dr. Hadi Sutanto)	(Assoc. Prof. Dr. Ganwarich pluphrach)
	……………………………. Committee
	(Prof. Dr. Hadi Sutanto)
	……………………………. Committee
	(Assoc. Prof. Dr. Paisarn Naphon)
	……………………………. Committee
	(Asst. Prof. Dr. Pracha Bunyawanichakul)

ACKNOWLEDGEMENTS

I would like to express sincere thanks to my advisor, Assoc. Prof. Dr .Ganwarich Phulphrach and Prof. Dr. Hadi Sutanto, for their valuable suggestions, attentive interest, and I would like to express sincere thanks to Asst. Prof. Dr. Wirat Chomkhuan, Asst. Prof. Charnont Moolwan and Dr.Samroeng Netpu’s kind recommendations in the present study. Sincere thanks to the members of my committee for their valuable time and suggestions. I am very grateful to the Department of Mechanical Engineering Srinakharinwirot University, Toyota automotive technological collage for providing the support for this thesis. Moreover, I would like to thank National metal and materials technology center (MTEC), for their help and guidance during my study. Lastly, I would like to thank my family for their support, encouragement, endless love and understanding throughout my study program.

Visanu Boonmag.

TABLE OF CONTENTS

TABLE OF CONTENTS (continued)

LIST OF TABLES

LIST OF FIGURES

LIST OF FIGURES (continued)

Figure **Page**

LIST OF FIGURES (continued)

Figure **Page**

LIST OF FIGURES (continued)

Figure **Page**

CHAPTER 1

INTRODUCTION

1 Overview

The helical gears are part of the transmission system in an automobile, to transmit power and motion from one to another parallel shaft. Failure of gears results in replacement parts and increased cost. For example, in this case, the pickup has to adjust the engine to increase horsepower. The transmission system was not designed for the higher torque. This results in a fracture in the helical gear in the 5^{th} position during the change from gear of 4^{th} to 5^{th} position. The helical gears made from chromium steel (JIS-SCr 420/AISI 5120) and more process of heat treatment.

The causes of gear failure are numerous including faulty design, improper applications, and manufacturing errors. Design errors include such things as incorrect gear geometry, incorrect material, poor material quality, and inadequate lubrication system. Application errors include things such as improper mounting and installation, inadequate cooling, improper lubrication, and poor maintenance. Manufacturing errors could be poor machining or faulty heat treatment of parts or poor gear system assembly.

Most of that damage is caused by a fracture of the teeth reacting with bending stresses. This phenomenon is called (pitting) or the holes on the gear teeth which stress exposed at the surface due to the backlash (contact stress). Analysis of the bending stresses and contact stress is used in several methods. Analysis of the bending stresses by AGMA bending equation and contact stresses by AGMA contact equation, both methods show difficulty. Another better method is finite element method which can simulate the stresses induced in the teeth flank, teeth fillet during meshing of gears. Because of the above, this is the source of the breakage problem with the helical gears and using any tools to analyze the objective of the research is to study chemical properties, mechanical properties, microstructure and analytical method bending stress uses Lewis equation of AGMA standards and contact stress uses Hertz equation of AGMA standards and the results were compared with finite element method. These are all tools that are used widely in the automotive industry.

This paper aims to identify the causes of failure in a helical gear used in a pick-up car. The knowledge gained from this investigation would help prevent or minimize the reoccurrence of similar failures in the future.

2 Assumption

Factors affecting failure of the helical gears (Chemical composition, dimension of gears, torque, crack, speed, bending stress and contact stress) are critical for the mechanical properties of the harden chromium steel gears (JIS-SCr 420)

3 Objective

3.1 To analyze physical and mechanical property of a helical gear transmission pickup car.

3.2 To analyze bending and contact stresses of a helical gear transmission of pickup car using finite element method.

4 Scope

This research aims to analyze failure of helical gears that are made of harden chromium steel gears (JIS-SCr 420) is following as.

4.1 Chemical composition analysis.

4.2 Mechanical property of gear.

4.3 Analysis of bending stresses by AGMA bending equation and contact stresses by AGMA contact equation.

4.4 Analysis bending stress and contact stress using finite element method.

4.5 To compare the result between mechanical test and finite element method.

CHAPTER 2

LITERATURE REVIEW AND THEORY

1. Literature Review

Sermsak Kateboonlue (2002), Analysis of the stress distribution in spur and helical gear teeth by the finite element method. Analysis of stresses in spur and helical gear by using the theoretical equation compare a finite element method. Based on the results obtained from the finite element analysis and the theoretical equations, namely, Lewis equation and AGMA standard, it was found that the maximum bending stresses were found to be at the radius of gear fillets. The relationships between the bending stress and the corresponding dependent parameters; namely, diametral pitch, face width, gear ratio and transmitted power were also determined by using the data obtained from the finite element analysis and the theoretical equations, namely, Lewis equation and AGMA standard. Based on the results, it was found that those relationships were identical.

Anat Hasap (2005), Wear characteristics of miniature spur gear in high precision transmission systems. Experiment with the wear of spur gears in high precision transmission system which consists of a small gear made from materials in the polymer poly bromide and Poly ox methylene. Study the impact of various factors as affecting the wear of the small gear such torque, speed of operating conditions and the relationship of various factors on the wear of the small gear. The results of this study can be used as models for the design and applications for spur gears in high precision transmission system.

Osman Asi (2005), Fatigue failure of a helical gear in a gearbox. This paper presents a failure analysis of a helical gear used in gearbox of a bus, which is made from AISI 8620 steel. The helical gear had been in service about three years when several teeth failed. The failed helical gear had a number of adjacent teeth and random teeth breakage at one end of the teeth. An evaluation of the failed helical gear was undertaken to assess its integrity that included a visual examination, photo documentation, chemical analysis, micro-hardness measurement, and metallographic examination. The failure zones were examined with the help of a scanning electron microscope equipped with EDX facility. Results indicate that teeth of the helical gear failed by fatigue with a fatigue crack initiation from destructive pitting and spalling region at one end of tooth in the vicinity of the pitch line because of misalignment.

Samroeng Netpu, Panya Srichandr (2012), Failure analysis of a helical gear in a gearbox used in a steel rolling mill. This paper reports the results of an investigation into the premature failure of a helical gear used in a gearbox of a steel mill in Thailand. The gear failed after about 15,000 h of service which was much shorter than the normal service life of 40,000-50,000 h. It was concluded the helical gear subsequently failed due to fatigue fracture initiated by surface and subsurface damages resulting from excessive contact stress. Excessive contact stress at gear tooth surface resulted from the replacement of a new, more powerful motor. The lesson learned from this case is that one must be careful when replacing key components of machines. The consequences of any replacements must first be thoroughly analysed before the final decisions are made.

Charnont Moolwan, Samroeng Netpu (2012), Failure analysis of a two high gearbox shaft. This paper reports the results of failure analysis of a two high gearbox shaft of a gearbox in a hot steel rolling mill in Thailand which fail prematurely after about 15,000 hours of service. Standard procedures for failure analysis were employed in this investigation. The results showed that the shaft failed by fatigue fracture. Beach marks on the fracture surface were clearly visible. Fatigue cracks were initiated at the corners of the wobbler. Relatively small final fracture area of the fracture surface indicated that the shaft was under a low stress at the time of failure. It is concluded that the shaft failed by fatigue fracture and that premature failure occurred due to high stress concentration at the corners of the wobbler of the shaft which led eventually to fatigue crack initiation, crack growth, and final fracture. Improved design and machining practice suggested that this would help prolong service life of the component.

Govind T Sarkar, Yogesh L Yenarkar, Dipak V Bhope (2013), Stress analysis of helical gear by finite element method. The bending and surface stresses of gear tooth are major factor for failure of gear. Pitting is a surface fatigue failure due to repetitions of high contact stresses. This paper investigates finite element model for monitoring the stresses induced of tooth flank, tooth fillet during meshing of gears. The involute profile of helical gear has been modeled and the simulation is carried out for the bending and contact stresses and the same have been estimated. To estimate bending and contact stresses, 3D models for different helical angle, face width are generated by modeling software and simulation is done by finite element software packages. Analytical methods of calculating gear bending stresses uses AGMA bending equation and for contact stress AGMA contact equation are used. It is important to develop appropriate models of contact element and to get equivalent result using Ansys and compare the result with standard AGMA stress.

Samroeng Netpu, Panya Srichandr (2013), Failure analysis of a helical gear in power plant. This paper reports the results of failure analysis of failure analysis of a helical gear used in a power plant in Thailand. The gear failed after approximately nine years of service. Visual inspection as well as macro and microscopic examinations of fracture surface were performed. Microstructure of the gear material was examined and microanalysis were carried out. Microhardness at the case of the gear at various distances from the surface were measured. The results showed that the fracture surface exhibited fatigue fracture characteristics. There were inclusions in the microstructure of gear material. Microanalysis results indicated that the inclusions are iron oxide surrounded by (FeMo)3C carbide. It is concluded that the gear failed by fatigue fracture. The inclusion were thought to be formed during the casting of the ingot that was used to make the gear blank, possibly due to inadequate degassing or deoxidation of liguid steel prior to ingot casting.

J. Venkatesh, Mr. P. B. G. S. N. Murthy (2014), Design and structural analysis of high speed helical gear using Ansys. In the gear design the bending stress and surface strength of the gear tooth are considered to be one of the main contributors for the failure of the gear in a gear set. Thus, the analysis of stresses has become popular as an area of research on gears to minimize or to reduce the failures and for optimal design of gears In this paper bending and contact stresses are calculated by using analytical method as well as Finite element analysis. To estimate bending stress modified Lewis beam strength method is used. Pro-e solid modeling software is used to generate the 3-D solid model of helical gear. Ansys software package is used to analyze the bending stress. Contact stresses are calculated by using modified AGMA contact stress method. In this also Pro-e solid modeling software is used to generate contact gear tooth model. Ansys software package is used to analyze the contact stress. Finally these two methods bending and contact stress results are compared with each other.

2. Theory

2.1 Gearing material

Alloyed steel to JIS G 4053 case hardening steels standard grade SCr 420 (AISI-5120) for applications requiring high tensile strength and toughness values, in particular in medium and large cross sections in the quenched and tempered condition. The chemical composition of SCr 420 alloy steel as shows in table 1.

Table 1 Chemical composition for chromium steel SCr 420. (From JIS G 4053. (2003). Japanese Industrial Standard. First English Edition. Japan)

Typical analysis	C	Si	Mn	P	S	Ni	Cr
(Ave. values %)	0.18-0.23	0.15-0.35	0.60-0.90	≤ 0.030	≤ 0.030	≤ 0.025	0.90-1.20

SCr 420- alloyed case hardening steel for parts with a required core tensile strength of 1000 - 1300 N/mm² and good wearing resistance as boxes, piston bolts, spindles, camshafts, gears, shafts and other mechanical controlling parts. The heat treatments and mechanical properties of SCr 420 steel look at table 2 – 3. The details are obtained in Appendix B.

Table 2 Heat treatments of SCr 420 alloy steel. (From Saarstahl. Material Specification Sheet. URL: http//www.saarstahl.com)

Forging	Commence 1100 - 850°C
Normalizing	Heat to approx. 840 - 870˚C, furnace cooling
Soft annealing	Heat to approx. 650 - 700°C/furnace
Carburising	Heat to approx. 880 - 980°C
Core hardening	Heat to approx. 860 - 900°C/oil
Case hardening	Heat to approx. 780 - 820°C/oil
Tempering	Heat to approx. 150 - 200°C, water cooling

Table 3 Mechanical properties of SCr 420 alloy steel. (From Saarstahl. Material Specification Sheet. URL: http//www.saarstahl.com)

Tensile Strength N/mm^2	1000 - 1300
Modulus of elasticity 10^3 N/mm^2	210
Brinell hardness (HBW): (+TH)	170 – 217 HB
Percentage of elongation %	8% minimum
Reduction Ratio	Minimum 3.5:1

The microstructure of case carburized and tempered specimen of SCr420 steel as shown in Figure 1, the metallographic observations perform revealed the presence of fine pearlitic microstructures with inter lamellar spacing on the order of 20 µm. When viewed at high magnification, deep-penetrating grain boundary oxides could be observed in the outermost layers of polished and etched specimens, as shown in Figure 2. In order to ascertain the depth of oxide formation, the specimens were polished lightly after etching with Nital.

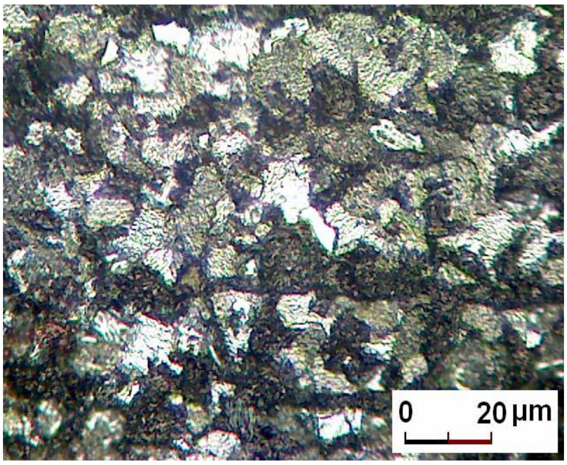

Figure 1 Metallograph of SCr420 steel (etched in 3% Nital for 4 seconds) in green state revealing the presence of pearlitic microstructure. (From *Dry Sliding Wear Behavior of Carburized 20mncr5 Alloy Steel*, International Journal of Engineering Science Invention,Vol. 3, 2014)

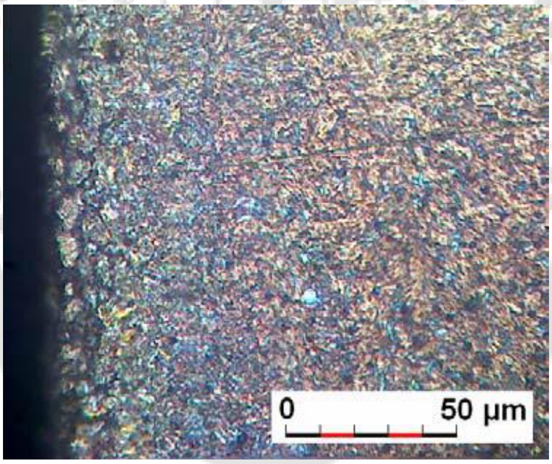

Figure 2 Micrographs indicating the presence of internal oxidation in SCr420 specimens etched in 3% Nital for 5 seconds**.** (From *Dry Sliding Wear Behavior of Carburized 20mncr5 Alloy Steel*, International Journal of Engineering Science Invention, Vol.3, 2014)

2.2 Carburizing of gears

This is the oldest and one of the cheapest methods of case hardening. A low-carbon steel, usually about 0.20 percent carbon or lower, is placed in an atmosphere that contains substantial amounts of carbon monoxide. The usual carburizing temperature is

1700^{o}F. The carburizing process diffuses carbon into the surface of heat-treated components in an atmosphere controlled furnace followed by directly quenching the processed gears into a selected quenchant thus introducing high carbon quenched, hard martensite case. Commercial carburizing may be accomplished by means of pack carburizing, gas carburizing, and liquid carburizing.

2.2.1 Pack carburizing

In pack carburizing, the work is surrounded by a carburizing compound in a closed container. The container is heated to the proper temperature for the required amount time and then slow-cooled. This is essentially a batch method and does not lend itself to high production. Commercial carburizing compounds usually consist of hardwood charcoal, coke, and about 20 percent of barium carbonate as an energizer. The carburizing compound is in the form of coarse particles or lumps, so that, when the cover is sealed on the container, sufficient air will be trapped inside to form carbon monoxide. The principal advantages of pack carburizing are that it does not require the use of a prepared atmosphere and that it is efficient and economical for individual processing of small lots of parts or of large, massive parts. The disadvantages are that It is not well suited to the production of thin carburized cases that must be controlled to close tolerances; it Cannot provide the close control of surface carbon that can be obtained by gas carburizing; parts cannot be direct-quenched from the carburizing temperature; and excessive time is consumed in heating and cooling the, charge. Because of the inherent variation in case depth and the cost of packing materials, pack carburizing is not used on work requiring a case depth of less than 0.030 in. and tolerances are at least 0.010 in.

2.2.2 Liquid carburizing

Liquid carburizing is a method of case hardening steel by placing it in a bath of molten cyanide so that carbon will diffuse from the bath in to the metal and produce a case comparable to the one resulting from pack or gas carburizing. Liquid carburizing may be distinguished from cyaniding by the character and composition of the case produced. The cyanide case is higher in nitrogen and lower in carbon the reverse is true of liquid carburized cases. Low temperature salt baths (lights case) usually contain a cyanide content of 20 percent and operate between 1550 °F and 1650° F. High temperature salt baths (deep case) usually have cyanide content of 10 percent and operate between 1650°F and 1750° F.

2.2.3 Gas carburizing

Gas carburizing consists of heating and holding low carbon alloy steel (0.07-0.28 percent Carbon) at normally 1650–1800°F (899–982°C) in a controlled atmosphere which causes additional carbon to diffuse into the steel (typically 0.70-1.10 percent carbon at the surface). Gear blanks to be carburized and hardened are generally preheated after the initial anneal by a subcritical anneal at 1100 °F-1250°F (590–675°C), normalize, normalize and temper or quench and temper to specified hardness before carburize hardening. This is done for machinability, dimensional stability and possible grain refinement considerations. An intermediate stress relief before final machining before carburizing may be used to remove residual stress from rough machining. After carburizing for the appropriate time, gearing will usually be cooled to 1475-1550°F (802–843°C), held at temperature to stabilize while maintaining the carbon potential, and direct quenched. Gearing may be atmosphere cooled after carburizing to below approximately 600°F (315°C) and then reheated in controlled atmosphere to 1475-1550°F (802-843°C) and quenched. After quenching, gearing is usually tempered at 300–375°F (149–191°C). Gearing may be subsequently given a refrigeration treatment to transform retained austenite and retempered.

2.3 Failure analysis

The failure of engineering materials is almost always an undesirable event for several reasons; these include human lives that are put in jeopardy, economic losses, and the interference with the availability of products and services. Even though the causes of failure and the behavior of materials may be known, prevention of failures is difficult to guarantee. The usual causes are improper materials selection and processing and inadequate design of the component or its misuse. It is the responsibility of the engineer to anticipate and plan for possible failure and, in the event that failure does occur, to assess its cause and then take appropriate preventive measures against future incidents. The following topics are simple fracture ductile and brittle modes. These discussions include failure mechanisms and methods by which failure may be prevented or controlled.

2.3.1 Ductile fracture

Ductile fracture surfaces will have their own distinctive features on both Macroscopic and microscopic levels. Figure 3 shows schematic representations for two characteristic macroscopic fracture profiles. The configuration shown in Figure 3*a* is found for extremely soft metals, such as pure gold and lead at room temperature, and other metals, polymers, and inorganic glasses at elevated temperatures. These highly ductile materials neck down to a point fracture, showing virtually 100% reduction in area.

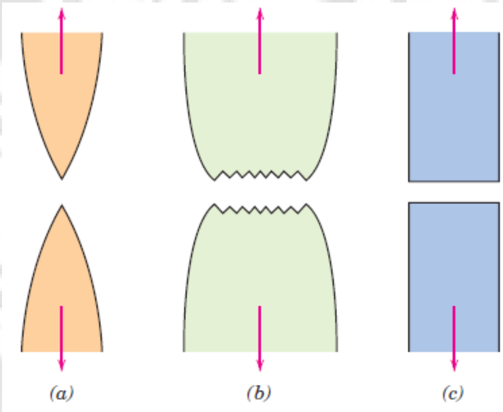

Figure 3 (*a*) Highly ductile fracture in which the specimen necks down to a point. (*b*) Moderately ductile fracture after some necking. (*c*) Brittle fracture without any plastic deformation. (From William D. Callister, Jr., *Materials Science and Engineering an Introduction Failure*, Seventh edition, Copyright 2007 by John Wiley & Sons, Inc

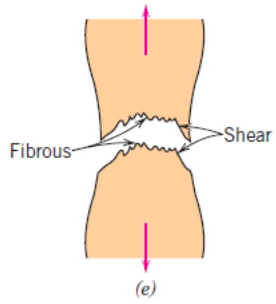

Figure 4 Stages in the cup-and-cone fracture. (*a*) Initial necking. (*b*) Small cavity formation. (*c*) Coalescence of cavities to form a crack. (*d*) Crack propagation. (*e*) Final shear fracture at a angle relative to the tensile direction. (From K. M. Ralls, T. H. Courtney, and J.Wulff, *Introduction to Materials Science and Engineering,* p. 468. Copyright © 1976 by John Wiley & Sons, New York. Reprinted by permission of John Wiley & Sons, Inc.)

The most common type of tensile fracture profile for ductile metals is that represented in Figure 3*b*, where fracture is preceded by only a moderate amount of necking. The fracture process normally occurs in several stages (Figure 4). First, after necking begins, small cavities, or microvoids, form in the interior of the cross section, as indicated in Figure 4*b*. Next, as deformation continues, these microvoids enlarge, come together, and coalesce to form an elliptical crack, which has its long axis perpendicular to the stress direction. The crack continues to grow in a direction parallel to its major axis by this microvoid coalescence process (Figure 4*c*). Finally, fracture ensues by the rapid propagation of a crack around the outer perimeter of the neck (Figure 4*d*), by shear deformation at an angle of about with the tensile axis-this is the angle at which the shear stress is a maximum. Sometimes a fracture having this characteristic surface contour is termed a *cup-and-cone fracture* because one of the mating surfaces is in the form of a cup, the other like a cone. In this type of fractured specimen (Figure 5*a*), the central interior region of the surface has an irregular and fibrous appearance, which is indicative of plastic deformation.

Figure 5 (*a*) Cup-and-cone fracture in aluminum. (*b*) Brittle fracture in a mild steel. (From William D. Callister, Jr., *Materials Science and Engineering an Introduction Failure*, Seventh edition, Copyright 2007 by John Wiley & Sons, Inc.)

Much more detailed information regarding the mechanism of fracture is available from microscopic examination, normally using scanning electron microscopy. Studies of this type are termed *fractographic*. The scanning electron microscope is preferred for fractographic examinations since it has a much better resolution and depth of field than does the optical microscope; these characteristics are necessary to reveal the topographical features of fracture surfaces.

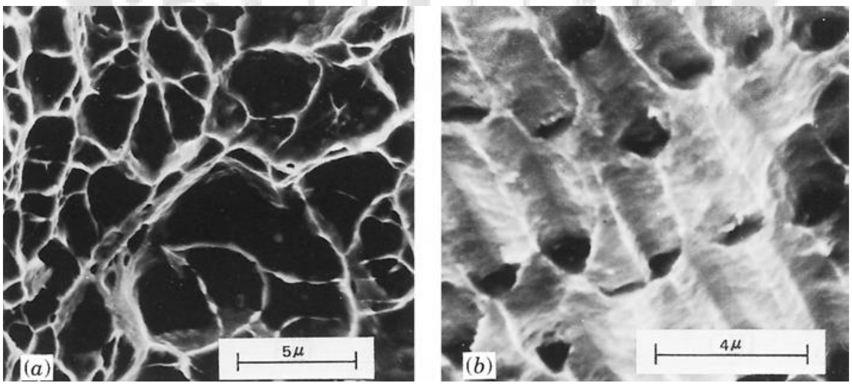

Figure 6 (*a*) Scanning electron fractograph showing spherical dimples characteristic of ductile fracture resulting from uniaxial tensile loads. 3300x. (*b*) Scanning electron fractograph showing parabolic-shaped dimples characteristic of ductile fracture resulting from shear loading. 5000x. (From R.W. Hertzberg, *Deformation and Fracture Mechanics of Engineering Materials,* 3rd edition. Copyright © 1989 by John Wiley & Sons, New York. Reprinted by permission of John Wiley & Sons, Inc.)

When the fibrous central region of a cup-and-cone fracture surface is examined with the electron microscope at a high magnification, it will be found to consist of numerous spherical “dimples” (Figure 6*a*); this structure is characteristic of fracture resulting from uniaxial tensile failure. Each dimple is one half of a microvoid that formed and then separated during the fracture process. Dimples also form on the shear lip of the cup-and-cone fracture. However, these will be elongated or C-shaped, as shown in Figure 6*b*. This parabolic shape may be indicative of shear failure. Furthermore, other microscopic fracture surface features are also possible. Fractographs such as those shown in Figure 6*a* and 6*b* provide valuable information in the analyses of fracture, such as the fracture mode, the stress state, and the site of crack initiation.

2.3.2 Brittle fracture

Fracture surfaces of materials that failed in a brittle manner will have their own distinctive patterns; any signs of gross plastic deformation will be absent. For example, in some steel pieces, a series of V-shaped “chevron” markings may form near the center of the fracture cross section that point back toward the crack initiation site (Figure 7*a*). Other brittle fracture surfaces contain lines or ridges that radiate from the origin of the crack in a fanlike pattern (Figure 7*b*). Often, both of these marking patterns will be sufficiently coarse to be discerned with the naked eye. For very hard and fine-grained metals, there will be no discernible fracture pattern. Figure 8, a micrograph of the center of axle specimen reveals the presence of cleavage features, which indicates that this was a brittle fracture.

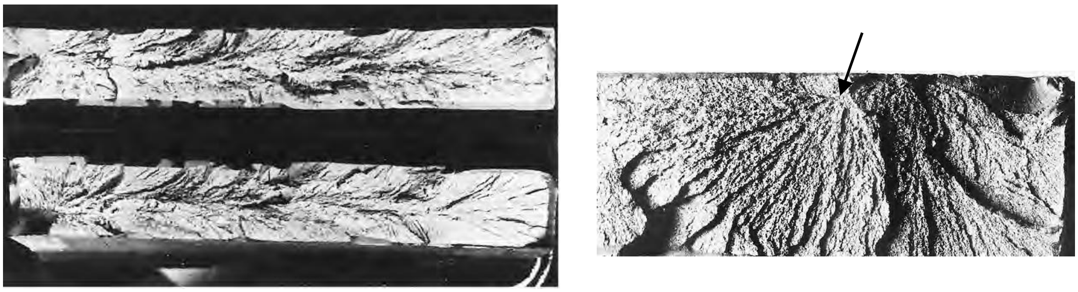

Figure 7 (*a*) Photograph showing V-shaped “chevron” markings characteristic of brittle fracture. Arrows indicate origin of crack. Approximately actual size. (*b*) Photograph of a brittle fracture surface showing radial fan-shaped ridges. Arrow indicates origin of crack. Approximately 2x. ((*a*) From R.W. Hertzberg, *Deformation and Fracture Mechanics of Engineering Materials,* 3rd edition. Copyright © 1989 by John Wiley & Sons, New York. Reprinted by permission of John Wiley & Sons, Inc. Photograph courtesy of Roger Slutter, Lehigh University. (*b*) Reproduced with permission from D. J.Wulpi, *Understanding How Components Fail,* American Society for Metals, Materials Park, OH, 1985.)

For most brittle crystalline materials, crack propagation corresponds to the Successive and repeated breaking of atomic bonds along specific crystallographic planes (Figure 9*a*); such a process is termed *cleavage*. This type of fracture is said to be **transgranular** (or *transcrystalline*), because the fracture cracks pass through the grains. Macroscopically, the fracture surface may have a grainy or faceted texture (Figure 9*b*), as a result of changes in orientation of the cleavage planes from grain to grain. This cleavage feature is shown at a higher magnification in the scanning electron micrograph of Figure 9*b*.

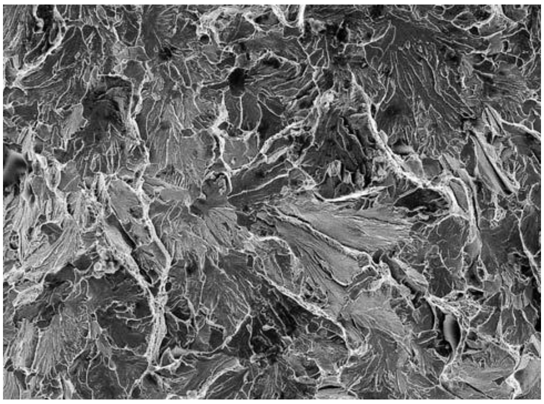

Figure 8 This area of cleavage fracture from the center of axle is typical of cleavage fracture. (From *Failure Analysis of Induction Hardened Automotive Axles,* Journal of Failure Analysis & Prevention, Vol. 8 (2008), Springer)

In some alloys, crack propagation is along grain boundaries (Figure 10*a*); this fracture is termed **intergranular.** Figure 10*b* is a scanning electron micrograph showing a typical intergranular fracture. This type of fracture normally results subsequent to the occurrence of processes that weaken or embrittle grain boundary regions.

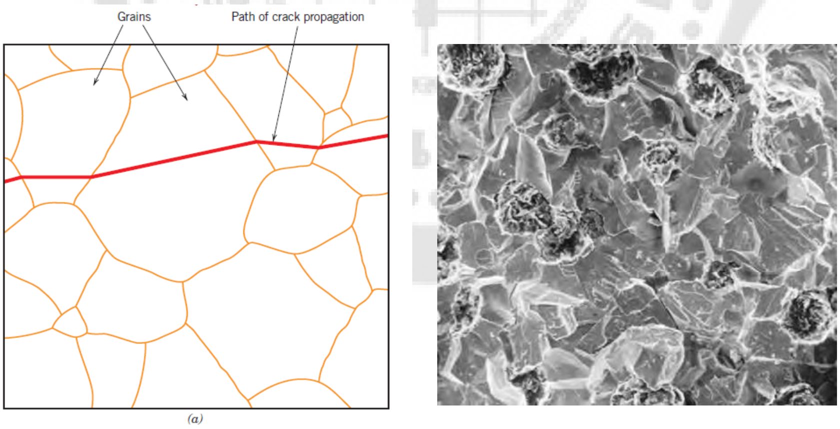

Figure 9 (*a*) Schematic cross-section profile showing crack propagation through the interior of grains for transgranular fracture. (*b*) Scanning electron fractograph of ductile cast iron showing a transgranular fracture surface. Magnification unknown. (Figure (*b*) from V. J. Colangelo and F. A. Heiser, *Analysis of Metallurgical Failures,* 2nd edition. Copyright © 1987 by John Wiley & Sons, New York. Reprinted by permission of John Wiley & Son.)

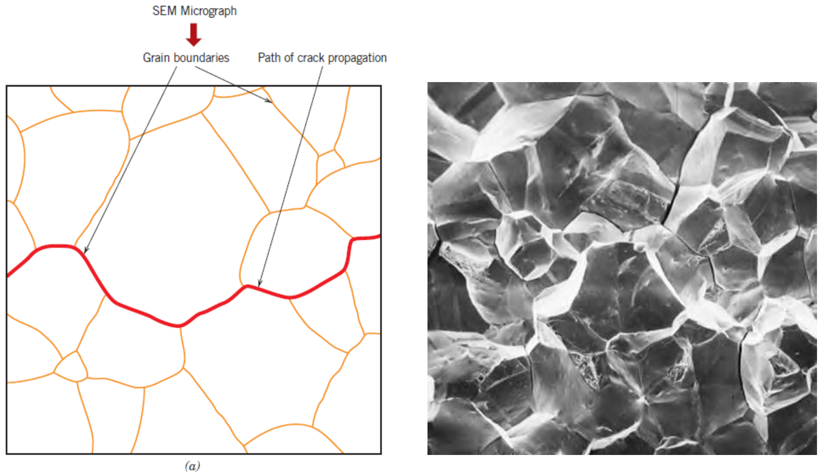

Figure 10 (*a*) Schematic cross-section profile showing crack propagation along grain boundaries for intergranular fracture. (*b*) Scanning electron fractograph showing an intergranular fracture surface. 50x. (Figure (*b*) reproduced with permission from *ASM Handbook,* Vol. 12, *Fractography,* ASM International, Materials Park, OH, 1987.)

2.4 Fundamentals of gear

The terminology of spur-gear teeth is illustrated in Figure 11. A pinion is the smaller of two mating gears. The larger is often called the driven gear.

The circular pitch p is the distance, measured on the pitch circle, from a point on one tooth to a corresponding point on an adjacent tooth. Thus the circular pitch is equal to the sum of the tooth thickness and the width of space.

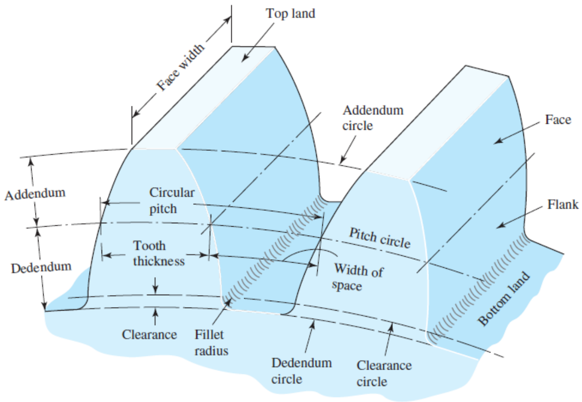

Figure 11 Nomenclature of spur-gear teeth (From Shigley's, *Mechanical engineering design*, Tenth edition, Copyright 2011 by the McGraw-Hill companies Inc., Reprinted by permission of the McGraw-Hill companies Inc.)

The module m is the ratio of the pitch diameter to the number of teeth. The customary unit of length used is the millimeter. The module is the index of tooth size in SI.

The diametral pitch P is the ratio of the number of teeth on the gear to the pitch diameter. Thus, it is the reciprocal of the module. Since diametral pitch is used only with U.S. units, it is expressed as teeth per inch.

The addendum (a) is the radial distance between the *top land* and the pitch circle. The dedendum *b* is the radial distance from the bottom land to the pitch circle. The *whole* depth ht is the sum of the addendum and the dedendum.

The clearance circle is a circle that is tangent to the addendum circle of the mating gear. The clearance c is the amount by which the dedendum in a given gear exceeds the addendum of its mating gear. The *backlash* is the amount by which the width of a tooth space exceeds the thickness of the engaging tooth measured on the pitch circles.

2.5 The Lewis bending equation

Wilfred Lewis introduced an equation for estimating the bending stress in gear teeth in which the tooth form entered into the formulation. The equation, announced in 1892, still remains the basis for most gear design today

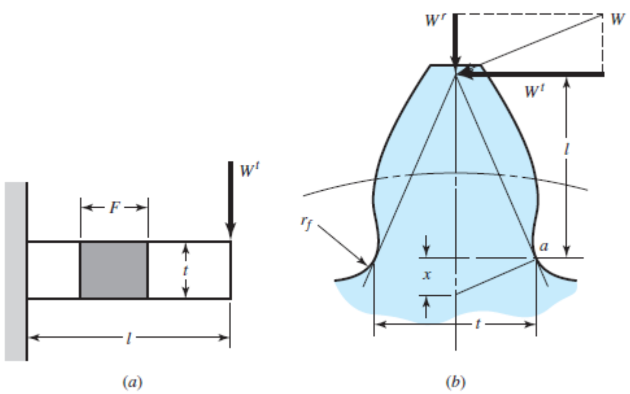

Figure 12 The maximum stress in a gear tooth. (From Shigley's, *Mechanical engineering design*, Tenth edition, Copyright 2015 by the McGraw-Hill companies Inc., Reprinted by permission of the McGraw-Hill companies Inc.)

To derive the basic Lewis equation, refer to Figure 12. Bending failure and pitting of the teeth are the two main failure modes in a transmission gearbox. The bending stresses in a helical gear are another interesting problem. When loads are too large, bending failure will occur. Bending failure in gears is predicted by comparing the calculated bending stress to experimentally-determined allowable fatigue values for the given material. This bending stress Equation (2-1) was derived from the Lewis formula. Bending Stress is given by

$$\sigma_b = \frac{W^t}{K_v b m_t Y_J} \tag{2-1}$$

Y_J called the Lewis form factor. The Lewis equation considers only static loading and does not take the dynamics of meshing teeth into account.

The maximum stress is expected at the point which is a tangential point where the parabola curve is tangent to the curve of the tooth root fillet called parabola tangential method. Two points can be found at each side of the tooth root fillet. The stress on the area connecting those two points is thought to be the worst case.

The AGMA equation for bending stresses given by,

$$\sigma_b = \frac{W^t K_o K_v K_s K_H K_B}{b m_t Y_J} \tag{2-2}$$

where for SI units, W^t is the tangential transmitted load (N), K_v is the dynamic factor, K_s is the size factor, K_B is the rim-thickness factor, *b* is the face width of the narrower member (mm), K_H is the load-distribution factor, K_o is the overload factor, m_t is the transverse metric module, Y_J is the geometry factor for bending strength.

2.5.1 Overload Factor K_o

The overload factor K_o is intended to make allowance for all externally applied loads in excess of the nominal tangential load W^t in a particular application see Table 4. Examples include variations in torque from the mean value due to firing of cylinders in an internal combustion engine or reaction to torque variations in a piston pump drive. There are other similar factors such as application factor or service factor. These factors are established after considerable field experience in a particular application.

Table 4 Overload Factor, K_o

Driven Machine			
Power source	Uniform	Moderate shock	Heavy shock
Uniform	1.00	1.25	1.75
Light shock	1.25	1.50	2.00
Medium shock	1.50	1.75	2.25

2.5.2 Size Factor K_s

The size factor reflects non-uniformity of material properties due to size. It depends upon Tooth size, Diameter of part, Ratio of tooth size to diameter of part, Face width, Area of stress attern, Ratio of case depth to tooth size and Hardenability and heat treatment. Standard size factors for gear teeth have not yet been established for cases where there is a detrimental size effect. In such cases AGMA recommends a size factor greater than unity. If there is no detrimental size effect, use unity. AGMA has identified and provided a symbol for size factor. Also, AGMA suggests K_s = 1.Noting that K_s is the reciprocal of K_b, we find the result of all the algebraic substitution is

$$K_s = \frac{1}{k_b} = 1.192\left(\frac{F\sqrt{Y}}{P}\right)^{0.0535} \qquad \text{(a)}$$

Table 5 Values of the Lewis Form Factor Y (These Values Are for a Normal Pressure Angle of 20^{o}, Full-Depth Teeth, and a Diametral Pitch of Unity in the Plane of Rotation)

Number of Teeth	Y	Number of Teeth	Y
12	0.245	28	0.353
13	0.261	30	0.359
14	0.277	34	0.371
15	0.290	38	0.384
16	0.296	43	0.397
17	0.303	50	0.409
18	0.309	60	0.422
19	0.314	75	0.435
20	0.322	100	0.447
21	0.328	150	0.460
22	0.331	300	0.472
24	0.337	400	0.480
26	0.346	Rack	0.485

K_s can be viewed as Lewis's geometry incorporated into the Marin size factor in fatigue. You may set K_s = 1, or you may elect to use the preceding Eq. (*a*). This is a point to discuss with your instructor. We will use Eq. (*a*) to remind you that you have a choice. If K_s in Eq. (*a*) is less than 1, use K_s = 1

2.5.3 Load-Distribution Factor K_H

The load-distribution factor modified the stress equations to reflect non-uniform distribution of load across the line of contact. The ideal is to locate the gear "midspan" between two bearings at the zero slope place when the load is applied. However, this is not always possible. The following procedure is applicable to

• Net face width to pinion pitch diameter ratio $\dfrac{F}{d_P} \le 2$

• Gear elements mounted between the bearings, Face widths up to 40 in

• Contact, when loaded, across the full width of the narrowest member

The load-distribution factor under these conditions is currently given by the face load distribution factor, C_{pf}, where

$$K_H = 1 + C_{mc}(C_{pf}C_{pm} + C_{ma}C_e) \tag{2-3}$$

where

$$C_{mc} = \begin{cases} 1 & \text{for uncrowned teeth} \\ 0.8 & \text{for crowned teeth} \end{cases} \tag{2-4}$$

$$C_{pf} = \begin{cases} \dfrac{F}{10d_p} - 0.025 & F \le 1 \text{ in} \\ \dfrac{F}{10d_p} - 0.037 + 0.0125F & 1 \le F \le 17 \text{ in} \\ \dfrac{F}{10d_p} - 0.1109 + 0.0207F - 0.000228F^2 & 17 \le F \le 40 \text{ in} \end{cases} \tag{2-5}$$

Note that for values of $F/(10d_P) < 0.05$, $F/(10d_P) = 0.05$ is used.

$$C_{pm} = \begin{cases} 1 & \text{for straddle-mounted pinion with } \dfrac{S_1}{S} < 0.175 \\ 1.1 & \text{for straddle-mounted pinion with } \dfrac{S_1}{S} \ge 0.175 \end{cases} \tag{2-6}$$

$$C_{ma} = A + BF + CF^2 \tag{2-7}$$

$$C_e = \begin{cases} 0.8 & \text{for gearing adjusted at assembly, or compatibility is improved by lapping, or both} \\ 1 & \text{for all other conditions} \end{cases} \tag{2-8}$$

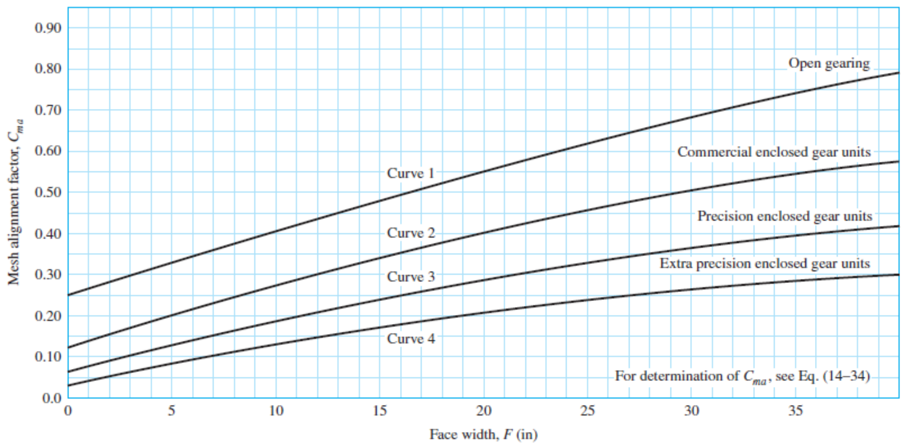

Figure 13 Mesh alignment factor C_{ma} . *(ANSI/AGMA 2001-D04.)*

2.5.4 Dynamic Factor K_v

As noted earlier, dynamic factors are used to account for inaccuracies in the manufacture and meshing of gear teeth in action. Transmission error is defined as the departure from uniform angular velocity of the gear pair. Some of the effects that produce transmission error are:

• Inaccuracies produced in the generation of the tooth profile; these include errors in tooth spacing, profile lead, and run out

• Vibration of the tooth during meshing due to the tooth stiffness

• Magnitude of the pitch-line velocity

• Dynamic unbalance of the rotating members

• Wear and permanent deformation of contacting portions of the teeth

• Gear shaft misalignment and the linear and angular deflection of the shaft

In an attempt to account for these effects, AGMA has defined a set of quality numbers, Q_v . These numbers define the tolerances for gears of various sizes manufactured to a specified accuracy. Quality numbers 3 to 7 will include most commercial quality gears. Quality numbers 8 to 12 are of precision quality. The following equations for the dynamic factor are based on these Q_v numbers:

$$K_v = \left(\frac{A+\sqrt{200V}}{A}\right)^B \qquad (2\text{-}9)$$

where A = 50 + 56(1 - B)

$$B = 0.25(12 - Q_v)^{2/3} \qquad (2\text{-}10)$$

2.5.5 Thickness Factor K_B

When the rim thickness is not sufficient to provide full support for the tooth root, the location of bending fatigue failure may be through the gear rim rather than at the tooth fillet. In such cases, the use of a stress-modifying factor K_B is recommended. This factor, the rim-thickness factor K_B, adjusts the estimated bending stress for the thin-rimmed gear.

Table 6 Reliability Factors $K_R\,(Y_Z)$ *Source: ANSI/AGMA 2001-D04.*

Reliability	$K_R\,(Y_Z)$
0.9999	1.50
0.999	1.25
0.99	1.00
0.90	0.85
0.50	0.70

2.5.6 Bending-Strength Geometry Factor Y_J

The AGMA factor J employs a modified value of the Lewis form factor, also denoted by Y; a fatigue stress-concentration factor K_f; and a tooth load-sharing ratio m_N. The load-sharing ratio m_N is equal to the face width divided by the minimum total length of the lines of contact. This factor depends on the transverse contact ratio m_P, the face-contact ratio m_F, the effects of any profile modifications, and the tooth deflection. For spur gears, m_N 5 1.0. For helical gears having a face-contact ratio m_F < 2.0, a conservative approximation is given by the equation

$$m_N = \frac{P_N}{0.95Z} \qquad (2\text{-}11)$$

where P_N is the normal base pitch and Y is the length of the line of action in the transverse plane.

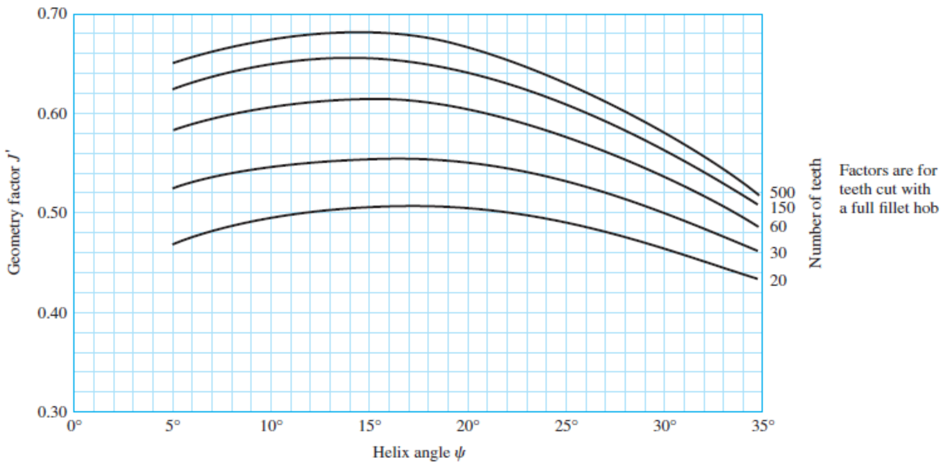

Figure 14 Helical-gear geometry factors J'. *Source:* The graph is from AGMA 218.01, which is consistent with tabular data from the current AGMA 908-B89. The graph is convenient for design purposes.

2.5.7 Surface-Strength Geometry Factor Z_I

The factor I is also called the *pitting-resistance geometry factor* by AGMA. We have replaced ϕ by ϕ_t, the transverse pressure angle, so that the relation will apply to helical gears too. Now define *speed ratio* m_G as

$$m_G = \frac{N_G}{N_P} \qquad (2\text{-}12)$$

The geometry factor Z_I for external spur and helical gears is the denominator adding the load-sharing ratio m_N, we obtain a factor valid for both spur and helical gears. The equation is then written as

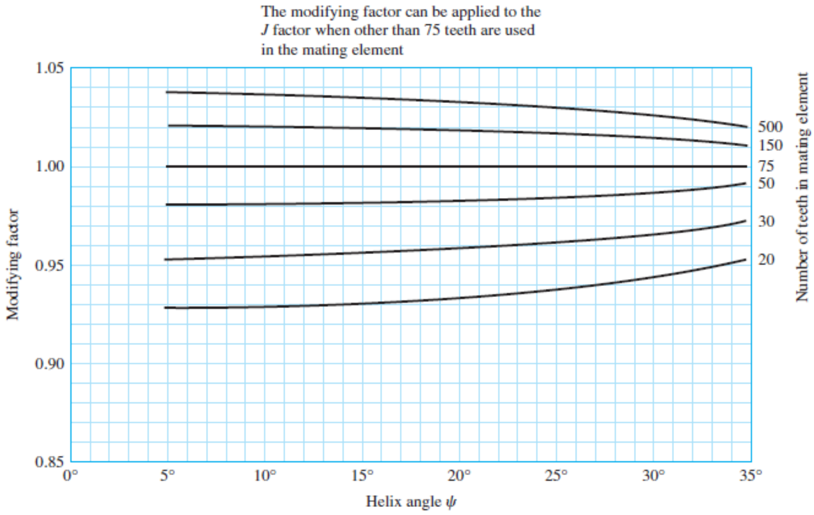

Figure 15 J'-factor multipliers for use with Figure 14 to find J . *Source:* The graph is from AGMA 218.01, which is consistent with tabular data from the current AGMA 908-B89.

The graph is convenient for design purposes.

$$Z_I = \begin{cases} \dfrac{\cos\phi_t \sin\phi_t}{2m_N}\dfrac{m_G}{m_G+1} & \text{external gears} \\ \\ \dfrac{\cos\phi_t \sin\phi_t}{2m_N}\dfrac{m_G}{m_G-1} & \text{internal gears} \end{cases} \tag{2-13}$$

where m_N = 1 for spur gears. In solving Eq. (2–11) for m_N , note that

$$P_N = P_n \cos\phi_n \tag{2-14}$$

where P_N is the normal circular pitch. The quantity *Z*, for use in Eq. (2–11), can be obtained from the equation

$$Z = \left[(r_p + a)^2 - r_{bP}{}^2\right]^{\frac{1}{2}} + \left[(r_G + a)^2 - r_{bG}{}^2\right]^{\frac{1}{2}} - (r_P + r_G)\sin\phi_t \tag{2-15}$$

where r_P and r_G are the pitch radii and r_{bP} and r_{bG} the base-circle radii of the pinion and gear, respectively.6 Recall from Eq. (13–6), the radius of the base circle is

$$r_b = r\cos\phi_t \tag{2-16}$$

2.5.8 The Elastic Coefficient Z_E

Values of Z_E may be computed directly from Table 7.

Table 7 Elastic Coefficient Z_E, 1psi (1MPa) *Source: AGMA 218.01*

		Gear Material and Modulus of Elasticity E_G, lbf/in^2 (MPa)					
Pinion Material	Pinion Modulus of Elasticity E_P Psi (MPa)	Steel 30 x 10^6 (2 x 10^5)	Malleable Iron 25 x 10^6 (1.7 x 10^5)	Nodular Iron 24 x 10^6 (1.7 x 10^5)	Cast Iron 22 x 10^6 (1.5 x 10^5)	Aluminum Bronze 17.5 x 10^6 (1.2 x 10^5)	Tin Bronze 16 x 10^6 (1.1 x 10^5)
Steel	30 x 10^6	2300	2180	2160	2100	1950	1900
	(2 x 10^5)	(191)	(181)	(179)	(174)	(162)	(158)
Malleable iron	25 x 10^6	2180	2090	2070	2020	1900	1850
	(1.7 x 10^5)	(181)	(174)	(172)	(168)	(158)	(154)
Nodular iron	24 x 10^6	2160	2070	2050	2000	1880	1830
	(1.7 x 10^5)	(179)	(172	(170)	(166)	(156)	(152)
Cast iron	22 x 10^6	2100	2020	2000	1960	1850	1800
	(1.5 x 10^5)	(174)	(168)	(166)	(163)	(154)	(149)
Aluminum	17.5 x 10^6	1950	1900	1880	1850	1750	1700
bronze	(1.2 x 10^5)	(162)	(158)	(156)	(154)	(145)	(141)
Tin bronze	16 x 10^6	1900	1850	1830	1800	1700	1650
	(1.1 x 10^5)	(158)	(154)	(152)	(149)	(141)	(137)

Poisson's ratio 5 0.30.

*When more exact values for modulus of elasticity are obtained from roller contact tests, they may be used.

2.6 The Hertz contact stress

One of the main gear tooth failure is pitting which is a surface fatigue failure due to repetition of high contact stresses occurring in the gear tooth surface while a pair of teeth is transmitting power. Contact failure in gears is currently predicted by comparing the calculated Hertz contact stress to experimentally determine allowable values for the given material. The method of calculating gear contact stress by Hertz's Equation (2-17) originally derived for contact between two cylinders.

In machine design, problems frequently occur when two members with curved surfaces are deformed when pressed against one another giving rise to an area of contact under compressive stresses. Of particular interest to the gear designer is the case where the curved surfaces are of cylindrical shape because they closely resemble gear tooth surfaces. The surface compressive stress (Hertzian stress) is found from the equation

$$\sigma_c = \sqrt{\frac{W_t}{\pi B\cos\phi} \times \frac{\frac{1}{r_1}+\frac{1}{r_2}}{\frac{1-{\nu_1}^2}{E_1}+\frac{1-{\nu_2}^2}{E_2}}} \tag{2-17}$$

$$r_1 = \frac{d_{p\sin\phi}}{2},\ r_2 = \frac{d_{p\sin\phi}}{2}$$

AGMA Contact Stress Equations

The fundamental equation for pitting resistance (contact stress) is

$$\sigma_c = Z_E \sqrt{\frac{W^t K_o K_v K_s K_H Z_R}{d_{w1} b Z_I}} \tag{2-18}$$

where for SI units, W^t is the tangential transmitted load (N), K_v is the dynamic factor, K_s is the size factor, *b* is the face width of the narrower member (mm), K_H is the load-distribution factor, K_o is the overload factor, Z_E is an elastic coefficient $\left(\sqrt{N/mm^2}\right)$, Z_R is the surface condition factor, d_{wl} is the pitch diameter of the pinion (mm) and Z_I is the geometry factor for pitting resistance.

2.7 Finite element method

2.7.1 General steps of the finite element method

Finite element method is a numerical method to approximate a given problem, with the appearance of the problem into smaller parts, called elements, these elements are connected together (Node) at a later point in the position to calculate the parameters desired (Dependent Variables) by creating an equation for each element corresponding to the differential equations of the problem. Then the equation will cause the solution to approximate with the finite element method and this will allow us to know the behavior of stress and strain, as well as moving around the various positions of the backlash. Current has developed a computer program used to calculate stress finite element method making it so easy and quick to find the stress in parts that we want to study. The analyst must make decisions that are carried out automatically by a computer program step 1-8 as following.

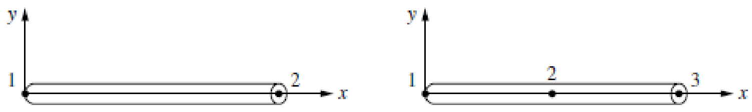

(a) Simple two-noded line element (typically used to represent a bar or beam element) and the higher-order line element

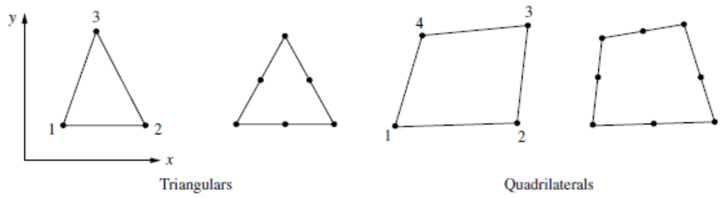

(b) Simple two-dimensional elements with corner nodes (typically used to represent plane stress/strain) and higher-order two-dimensional elements with intermediate nodes along the sides

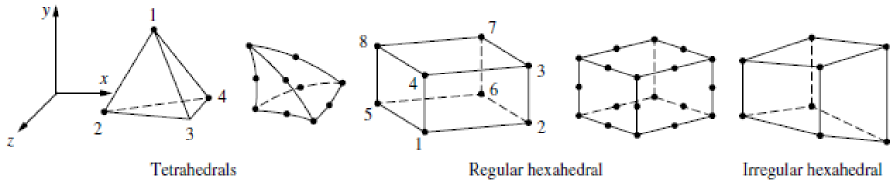

(c) Simple three-dimensional elements (typically used to represent three-dimensional stress state) and higher-order three-dimensional elements with intermediate nodes along edges

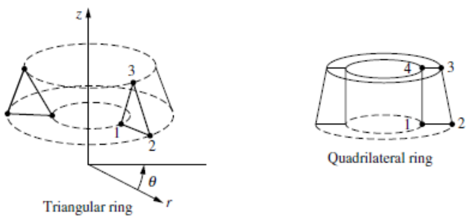

(d) Simple axisymmetric triangular and quadrilateral elements used for axisymmetric problems

Figure 16 Various types of simple lowest-order finite elements with corner nodes only and higher-order elements with intermediate nodes. (From Daryl L. Logan, *A First Course in the Finite Element Method*, Fourth Edition, Copyright 2007 by Thomson Canada Limited)

Step 1 Discretize and select the element types

Step 1 involves dividing the body into an equivalent system of finite elements with associated nodes and choosing the most appropriate element type to model more closely with the actual physical behavior. The total number of elements used and their variation in size and type within a given body are primarily matters of engineering judgment.

The elements must be made small enough to give usable results and yet large enough to reduce computational effort. Small elements (and possibly higher order elements) are generally desirable where the results are changing rapidly, such as where changes in geometry occur; large elements can be used where results are relatively constant.

The choice of elements used in a finite element analysis depends on the physical makeup of the body under actual loading conditions and on how close to the actual behavior the analyst wants the results to be. Judgment concerning the appropriateness of one-, two-, or three-dimensional idealizations is necessary. Moreover, the choice of the most appropriate element for a particular problem is one of the major tasks that must be carried out by the designer/analyst. Elements that are commonly employed in practice-most of which are considered in this text-are shown in Fig 2.16.

The primary line elements [Figure 16(a)] consist of bar (or truss) and beam elements. They have a cross-sectional area but are usually represented by line segments. In general, the cross-sectional area within the element can vary, but throughout this text it will be considered to be constant. The simplest line element (called a linear element) has two nodes, one at each end, although higher-order elements having three nodes [Figure 16(a)] or more (called quadratic, cubic, etc. elements).

The basic two-dimensional (or plane) elements [Figure 16(b)] are loaded by forces in their own plane (plane stress or plane strain conditions). They are triangular or quadrilateral elements. The simplest two-dimensional elements have corner nodes only (linear elements) with straight sides or boundaries, although there are also higher-order elements, typically with mid-side nodes [Figure 16(b)] (called quadratic elements) and curved sides. The elements can have variable thicknesses throughout or be constant.

The most common three-dimensional elements [Figure 16(c)] are tetrahedral and hexahedral (or brick) elements; they are used when it becomes necessary to perform a three-dimensional stress analysis. The basic three-dimensional elements have corner nodes only and straight sides, whereas higher-order elements with mid-edge nodes (and possible mid-face nodes) have curved surfaces for their sides [Figure 16(c)].

The axisymmetric element [Figure 16(d)] is developed by rotating a triangle or quadrilateral about a fixed axis located in the plane of the element through 360. This element can be used when the geometry and loading of the problem are axisymmetric.

Step 2 Select a displacement function

Step 2 involves choosing a displacement function within each element. The function is defined within the element using the nodal values of the element. Linear, quadratic, and cubic polynomials are frequently used functions because they are simple to work with in finite element formulation. However, trigonometric series can also be used. For a two-dimensional element, the displacement function is a function of the coordinates in its plane (say, the *x-y* plane). The functions are expressed in terms of the nodal unknowns (in the two-dimensional problem, in terms of an x and a y component). The same general displacement function can be used repeatedly for each element. Hence the finite element method is one in which a continuous quantity, such as the displacement throughout the body, is approximated by a discrete model composed of a set of piecewise-continuous functions defined within each finite domain or finite element.

Step 3 Define the strain / Displacement and stress / Strain relationships

Strain/displacement and stress/strain relationships are necessary for deriving the equations for each finite element. In the case of one-dimensional deformation, say, in the *x* direction, we have strain ε_x related to displacement *u* by

$$\varepsilon_x = \frac{d_u}{d_x} \qquad (2\text{-}19)$$

for small strains. In addition, the stresses must be related to the strains through the stress/strain law-generally called the constitutive law. The ability to define the material behavior accurately is most important in obtaining acceptable results. The simplest of stress/strain laws, Hooke's law, which is often used in stress analysis, is given by

$$\sigma_x = E\varepsilon_x \qquad (2\text{-}20)$$

Where are σ_x = stress in the *x* direction and *E* = modulus of elasticity.

Step 4 Derive the element stiffness matrix and equations

Initially, the development of element stiffness matrices and element equations was based on the concept of stiffness influence coefficients, which presupposes a background in structural analysis. We now present alternative methods used in this text that do not require this special background.

Direct Equilibrium Method, According to this method, the stiffness matrix and element equations relating nodal forces to nodal displacements are obtained using force equilibrium conditions for a basic element, along with force/deformation relationships. Because this method is most easily adaptable to line or one-dimensional elements, this method for spring, bar, and beam elements, respectively.

Work or Energy Methods, To develop the stiffness matrix and equations for two- and three-dimensional elements, it is much easier to apply a work or energy method. The principle of virtual work (using virtual displacements), the principle of minimum potential energy, and Castigliano's theorem are methods frequently used for the purpose of derivation of element equations.

Methods of Weighted Residuals, The methods of weighted residuals are useful for developing the element equations; particularly popular is Galerkin's method. These methods yield the same results as the energy methods wherever the energy methods are applicable. They are especially useful when a functional such as potential energy is not readily available. The weighted residual methods allow the finite element method to be applied directly to any differential equation.

Using any of the methods just outlined will produce the equations to describe the behavior of an element. These equations are written conveniently in matrix form as

$$\begin{Bmatrix} f_1 \\ f_2 \\ f_3 \\ . \\ . \\ f_n \end{Bmatrix} = \begin{bmatrix} k_{11} & k_{12} & k_{13} & \ldots & k_{1n} \\ k_{21} & k_{22} & k_{23} & \ldots & \\ k_{31} & k_{32} & k33 & \ldots & \\ . & . & . & . & . \\ . & . & . & . & . \\ k_{n1} & . & . & \ldots & k_{nn} \end{bmatrix} \begin{Bmatrix} d_1 \\ d_2 \\ d_3 \\ . \\ . \\ d_n \end{Bmatrix} \tag{2-21}$$

or in compact matrix form as

$$\{f\} = [k]\{d\} \tag{2-22}$$

Where $\{f\}$ is the vector of element nodal forces, $[k]$ is the element stiffness matrix (normally square and symmetric), and $\{d\}$ is the vector of unknown element nodal degrees of freedom or generalized displacements, *n*.

Step 5 Assemble the element equations to obtain the global or total equations and introduce boundary conditions.

In this step the individual element nodal equilibrium equations generated in step 4 are assembled into the global nodal equilibrium equations. Another more direct method of superposition (called the direct stiffness method), whose basis is nodal force equilibrium, can be used to obtain the global equations for the whole structure. Implicit in the direct stiffness method is the concept of continuity, or compatibility, which requires that the structure remain together and that no tears occur anywhere within the structure. The final assembled or global equation written in matrix form is

$$\{F\} = [K]\{d\} \tag{2-23}$$

Where $\{F\}$ is the vector of global nodal forces, $[K]$ is the structure global or total stiffness matrix, (for most problems, the global stiffness matrix is square and symmetric) and $\{d\}$ is now the vector of known and unknown structure nodal degrees of freedom or generalized displacements. It can be shown that at this stage, the global stiffness matrix $[K]$ is a singular matrix because its determinant is equal to zero. To remove this singularity problem, we must invoke certain boundary conditions (or constraints or supports) so that the structure remains in place instead of moving as a rigid body.

Step 6 Solve for the unknown degrees of freedom (or generalized displacements)

Equation (2-23), modified to account for the boundary conditions, is a set of simultaneous algebraic equations that can be written in expanded matrix form as

$$\begin{Bmatrix} F_1 \\ F_2 \\ . \\ . \\ F_n \end{Bmatrix} = \begin{Bmatrix} K_{11} & K_{12} & \ldots & K_{1n} \\ K_{21} & K22 & \ldots & K_{2n} \\ . & . & . & . \\ . & . & . & . \\ K_{n1} & K_{n2} & \ldots & K_{nn} \end{Bmatrix} \begin{Bmatrix} d_1 \\ d_2 \\ . \\ . \\ d_n \end{Bmatrix} \tag{2-24}$$

Step 7 Solve for the element strains and stresses

For the structural stress-analysis problem, important secondary quantities of strain and stress (or moment and shear force) can be obtained because they can be directly expressed in terms of the displacements determined in step 6. Typical relationships between strain and displacement and between stress and strain such as Equation (2-19) and (2-20) for one-dimensional stress given in step 3-can be used.

Step 8 Interpret the results

The final goal is to interpret and analyze the results for use in the design/analysis process. Determination of locations in the structure where large deformations and large stresses occur is generally important in making design/analysis decisions. Postprocessor computer programs help the user to interpret the results by displaying them in graphical form.

2.7.2 Applications of the finite element method

The finite element method can be used to analyze both structural and nonstructural problems. Typical structural areas

1. Stress analysis, including truss and frame analysis, and stress concentration problems typically associated with holes, fillets, or other changes in geometry in a body

2. Buckling

3. Vibration analysis

Finally, some biomechanical engineering problems (which may include stress analysis) typically include analyses of human spine, skull, hip joints, jaw/gum tooth implants, heart, and eye.

We now present some typical applications of the finite element method. These applications will illustrate the variety, size, and complexity of problems that can be solved using the method and the typical discretization process and kinds of elements used.

The finite element method used for this frame enables the designer/analyst quickly to obtain displacements and stresses in the tower for typical load cases, as required by design codes. Before the development of the finite element method and the computer, even this relatively simple problem took many hours to solve.

Another problem, that of the hydraulic cylinder rod end shown in Figure 17, was modeled by 120 nodes and 297 plane strain triangular elements. Symmetry was also applied to the whole rod end so that only half of the rod end had to be analyzed, Figure 18 illustrates the use of a three-dimensional solid element to model a swing casting for a backhoe frame. The three-dimensional hexahedral elements are necessary to model the irregularly shaped three-dimensional casting. Two-dimensional models certainly would not yield accurate engineering solutions to this problem.

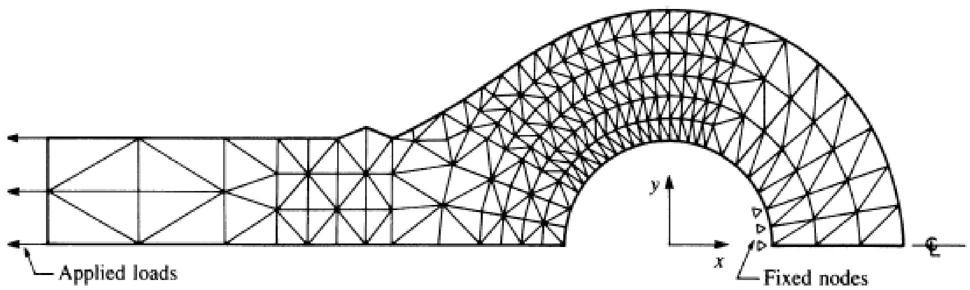

Figure 17 Two-dimensional analysis of a hydraulic cylinder rod end (120 nodes, 297 plane strain triangular elements) (From Daryl L. Logan, *A First Course in the Finite Element Method*, Fourth Edition, Copyright 2007 by Thomson Canada Limited)

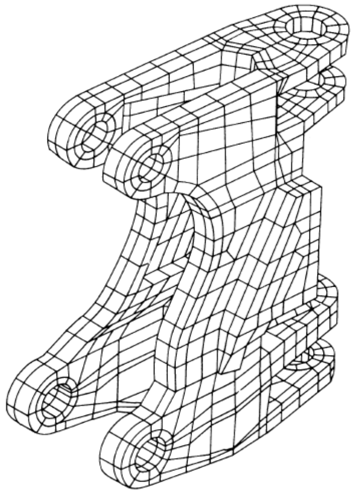

Figure 18 Three-dimensional solid element model of a swing casting for a backhoe frame. (From Daryl L. Logan, *A First Course in the Finite Element Method*, Fourth Edition, Copyright 2007 by Thomson Canada Limited)

2.7.3 Three-dimensional stress and strain

We begin by considering the three-dimensional infinitesimal element in Cartesian coordinates with dimensions *dx, dy,* and *dz* and normal and shear stresses as shown in Figure 19. This element conveniently represents the state of stress on three mutually perpendicular planes of a body in a state of three-dimensional stress. As usual, normal stresses are perpendicular to the faces of the element and are represented by

(a)

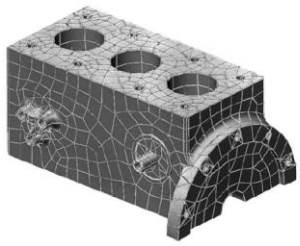

(b)

Figure 19 (a) wheel rim; (b) engine block. ((a) Courtesy of Mark Blair; (b) courtesy of Mark Guard.) (From Daryl L. Logan, *A First Course in the Finite Element Method*, Fourth Edition, Copyright 2007 by Thomson Canada Limited)

σ_x, σ_y, and σ_z. Shear stresses act in the faces (planes) of the element and are represented by τ_{xy}, τ_{yz}, τ_{zx}, and so on. From moment equilibrium of the element,

$$\tau_{xy} = \tau_{yx} \qquad \tau_{yz} = \tau_{zy} \qquad \tau_{zx} = \tau_{xz}$$

Hence, there are only three independent shear stresses, along with the three normal stresses.

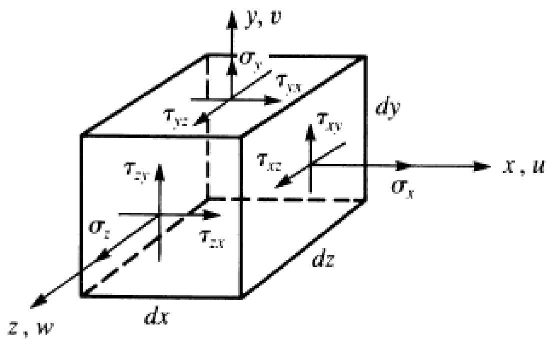

Figure 20 Three-dimensional stresses on an element. (From Daryl L. Logan, *A First Course in the Finite Element Method*, Fourth Edition, Copyright 2007 by Thomson Canada Limited)

They are repeated here, for convenience, as

$$\varepsilon_x = \frac{\partial u}{\partial x} \qquad \varepsilon_y = \frac{\partial v}{\partial y} \qquad \varepsilon_z = \frac{\partial w}{\partial z} \tag{2-25}$$

where *u, v,* and *w* are the displacements associated with the *x; y,* and *z* directions. The shear strains g are now given by

$$\begin{aligned} \gamma_{xy} &= \frac{\partial u}{\partial y} + \frac{\partial v}{\partial x} = \gamma_{yx} \\ \gamma_{yz} &= \frac{\partial v}{\partial z} + \frac{\partial w}{\partial y} = \gamma_{zy} \\ \gamma_{zx} &= \frac{\partial w}{\partial x} + \frac{\partial u}{\partial z} = \gamma_{xz} \end{aligned} \tag{2-26}$$

where, as for shear stresses, only three independent shear strains exist.

We again represent the stresses and strains by column matrices as

$$\{\sigma\} = \begin{Bmatrix} \sigma_x \\ \sigma_y \\ \sigma_z \\ \tau_{xy} \\ \tau_{yz} \\ \tau_{zx} \end{Bmatrix} \qquad \{\varepsilon\} = \begin{Bmatrix} \varepsilon_x \\ \varepsilon_y \\ \varepsilon_z \\ \gamma_{xy} \\ \gamma_{yz} \\ \gamma_{zx} \end{Bmatrix} \tag{2-27}$$

The stress/strain relationships for an isotropic material are again given by

$$\{\sigma\} = [D]\{\varepsilon\} \tag{2-28}$$

where $\{\sigma\}$ and $\{\varepsilon\}$ are defined by Eq. (2-28), and the constitutive matrix $[D]$ (see also Appendix C) is now given by

$$[D] = \frac{E}{(1+\nu)(1-2\nu)} \begin{bmatrix} 1-\nu & \nu & \nu & 0 & 0 & 0 \\ & 1-\nu & \nu & 0 & 0 & 0 \\ & & 1-\nu & 0 & 0 & 0 \\ & & & \frac{1-2\nu}{2} & 0 & 0 \\ & & & & \frac{1-2\nu}{2} & 0 \\ \text{Symmetry} & & & & \frac{1-2\nu}{2} & \end{bmatrix} \tag{2-29}$$

2.7.4 Tetrahedral element

Consider the tetrahedral element with corner nodes 1–4. This element is a 4 nodes solid shown in Figure 21 the principle are follows.

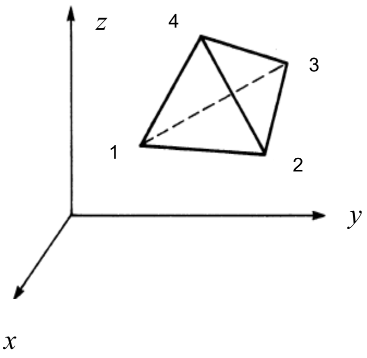

Figure 21 Tetrahedral solid elements (From Daryl L. Logan, *A First Course in the Finite Element Method*, Fourth Edition, Copyright 2007 by Thomson Canada Limited)

Assuming the distribution of solutions is estimated as follows.

$$\phi(x,y,z) = \alpha_1 + \alpha_2 x + \alpha_3 y + \alpha_4 z \qquad (2.30a)$$

where α_i, i = 1, 2, 3, 4 are constants determined by the conditions of the following 4 nodes which 4 fixed already. It can be written by the distributed nature of the approximate solution in terms of the nodes as follows.

$$\phi = N_1\phi_1 + N_2\phi_2 + N_3\phi_3 + N_4\phi_4 = \underset{(1x4)}{\lfloor N \rfloor} \underset{(4x1)}{\{\phi\}} \qquad (2.30b)$$

where N_i, i = 1, 2, 3, 4 is the shape function on the surface which can be written as follows.

. $$N_i = \frac{1}{6V}\left(a_i + b_i x + c_i y + d_i z\right) \qquad i = 1, 2, 3, 4 \qquad (2.30c)$$

Here in

$$V = \frac{1}{6}\begin{vmatrix} 1 & x_1 & y_1 & z_1 \\ 1 & x_2 & y_2 & z_2 \\ 1 & x_3 & y_3 & z_3 \\ 1 & x_4 & y_4 & z_4 \end{vmatrix} \qquad (2.30d)$$

$$a_1 = \begin{vmatrix} x_2 & y_2 & z_2 \\ x_3 & y_3 & z_3 \\ x_4 & y_4 & z_4 \end{vmatrix} \qquad c_1 = -\begin{vmatrix} x_2 & 1 & z_2 \\ x_3 & 1 & z_3 \\ x_4 & 1 & z_4 \end{vmatrix}$$

$$b_1 = -\begin{vmatrix} 1 & y_2 & z_2 \\ 1 & y_3 & z_3 \\ 1 & y_4 & z_4 \end{vmatrix} \qquad d_1 = -\begin{vmatrix} x_2 & y_2 & 1 \\ x_3 & y_3 & 1 \\ x_4 & y_4 & 1 \end{vmatrix} \qquad (2.30e)$$

where V = the volume of the tetrahedron and the other coefficients a_i, b_i, c_i, d_i, i = 2, 3, 4 are similar to equation (2.30e) which can be written by cyclic permutation.

2.7.5 Computer programs for the finite element method

There are two general computer methods of approach to the solution of problems by the finite element method. One is to use large commercial programs, many of which have been configured to run on personal computers (PCs); these general-purpose programs are designed to solve many types of problems. The other is to develop many small, special-purpose programs to solve specific problems. In this section, we will discuss the advantages and disadvantages of both methods. We will then list some of the available general-purpose programs and discuss some of their standard capabilities.

Some advantages of general-purpose programs:

1. The input is well organized and is developed with user ease in mind. Users do not need special knowledge of computer software or hardware. Preprocessors are readily available to help create the finite element model.

2. The programs are large systems that often can solve many types of problems of large or small size with the same input format.

3. Many of the programs can be expanded by adding new modules for new kinds of problems or new technology. Thus they may be kept current with a minimum of effort.

4. With the increased storage capacity and computational efficiency of PCs, many general-purpose programs can now be run on PCs.

5. Many of the commercially available programs have become very attractive in price and can solve a wide range of problems.

Some disadvantages of general-purpose programs:

1. The initial cost of developing general-purpose programs is high.

2. General-purpose programs are less efficient than special-purpose programs because the computer must make many checks for each problem, some of which would not be necessary if a special-purpose program were used.

3. Many of the programs are proprietary. Hence the user has little access to the logic of the program. If a revision must be made, it often has to be done by the developers.

Some advantages of special-purpose programs:

1. The programs are usually relatively short, with low development costs.

2. Small computers are able to run the programs.

3. Additions can be made to the program quickly and at a low cost.

4. The programs are efficient in solving the problems they were designed to solve.

The major disadvantage of special-purpose programs is their inability to solve different classes of problems. Thus one must have as many programs as there are different classes of problems to be solved.

There are numerous vendors supporting finite element programs, and the interested user should carefully consult the vendor before purchasing any software. However, to give you an idea about the various commercial personal computer programs now available for solving problems by the finite element method, we present a partial list of existing programs.

1. Algor

2. Abaqus

3. ANSYS

4. COSMOS/M

5. GT-STRUDL

6. MARC

7. MSC/NASTRAN

8. NISA

9. Pro/MECHANIC

10. SAP2000

11. STARDYNE

Standard capabilities of many of the listed programs are provided in the preceding references and in Reference [45]. These capabilities include information on

1. Element types available, such as beam, plane stress, and three dimensional solid

2. Type of analysis available, such as static and dynamic

3. Material behavior, such as linear-elastic and nonlinear

4. Load types, such as concentrated, distributed, thermal, and displacement (settlement)

5. Data generation, such as automatic generation of nodes, elements, and restraints (most programs have preprocessors to generate the mesh for the model)

6. Plotting, such as original and deformed geometry and stress and temperature contours (most programs have postprocessors to aid in interpreting results in graphical form)

7. Displacement behavior, such as small and large displacement and buckling

8. Selective output, such as at selected nodes, elements, and maximum or minimum values

All programs include at least the bar, beam, plane stress, plate-bending, and three dimensional solid elements, and most now include heat-transfer analysis capabilities. Complete capabilities of the programs are best obtained through program reference manuals and websites.

2.7 Assumption method

Assumption is a tool to investigate. If the first experimental observation is based on the hypothesis predicted. Researchers should not assume that the experimental results support that hypothesis. Please know that the hypothesis is only a temporary answer.

When there is clear evidence, assumptions can become a reality. When experimenting with the hypothesis. Researchers have determined that the hypothesis is canceled.

An investigation to answer the research is not a random event. It's proven to be systematic to evidence. As a result, the researchers were able to guess the answer, even if temporarily, study the problem in detail, use the hypothesis as a set of guidelines to find the answer. It also proposes a variable and experimental.

Assumption must have some kind of neutral. The assumption is just suggestions to make a point to find out why. So there are experiment and then results, They are interpreted that way. Hypothesis is true predictions, while there is no evidence that seemed to support, the assumption is that what is said about the relationship of two or more variables, the assumption must be that the relationship between the variables. The guidelines indicate that relationship. Therefore, identifying variables is making sure that there is no need to study variables. First of all, the traffic on the definition of a variable before. So there is understanding, which means the change of sign or the fact that both quantity and quality such as color, sex, year etc. Variables the researcher are made aware of are the relationships between concepts. Guide the formulation of hypotheses within the framework of the theory. Enabling the researchers to learn how to analyze the data and some statistics.

CHAPTER 3

MATERIAL AND EXPERIMENTAL METHODS

1. Material and experimental methods

This study was conducted on a failed helical gear used in a pick-up car. Composition (wt%) analysis, mechanical property, microstructure examination and finite element analysis of the failed gear was made from JIS-SCr 420 steel. The failure investigation was conducted as follows.

1.1 Chemical composition analysis

Chemical composition of the gear material was analyzed using an optical emission spectrometer (THERMO model ARL 3460) as shown in Figure 22. Specimens for microstructural examination were prepared in accordance with C E407 standard. Figure 23 shown the pinion gear side of the tracks through the electrons are 4 points at the outer surface region, and figure 24 shown the tracks through the electrons at the central region.

Figure 22 Spectrophotometer test machine (THERMO model ARL 3460).

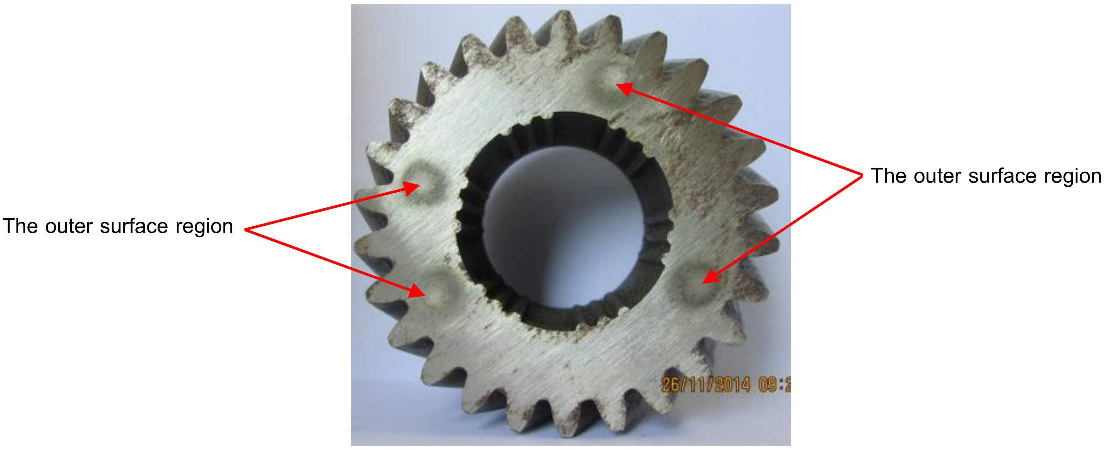

Figure 23 Pinion gear of the chemical examination by spectrometer at the outer surface region.

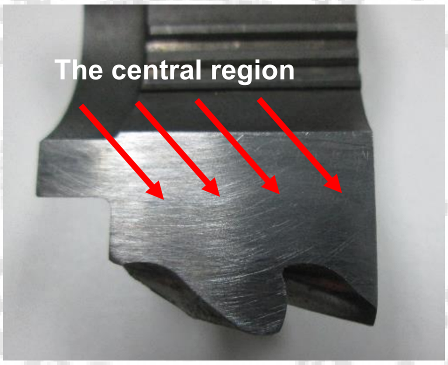

Figure 24 Pinion gear of the chemical examination by spectrometer at the central region.

1.2 Hardness measurements

Specimen was then sectioned for micro-hardness measurement, Micro-hardness was measured using (MITUTOYO: HM-210A) as shown in Figure 25, with diamond pyramid angle of 136^{o} indenter and 300 gm load. A total of 20 points as shown in Figure 26 were measured to establish the hardness profile of the case of the failed gear under ASTM E92-82 (Reapproved 2003).

Figure 25 Micro-Vickers hardness testing machines (MITUTOYO: HM-210A).

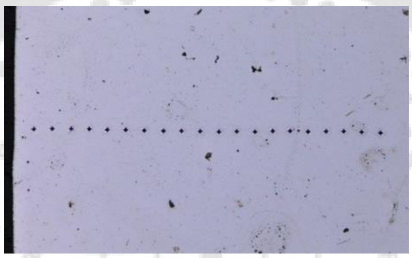

Figure 26 A total of 20 points with diamond pyramid from the outer to the central region.

1.3 Microstructure examination

Microstructure was examined using an optical microscope (Olympus laser microscopes model OLS 4000) as show in Figure 27.

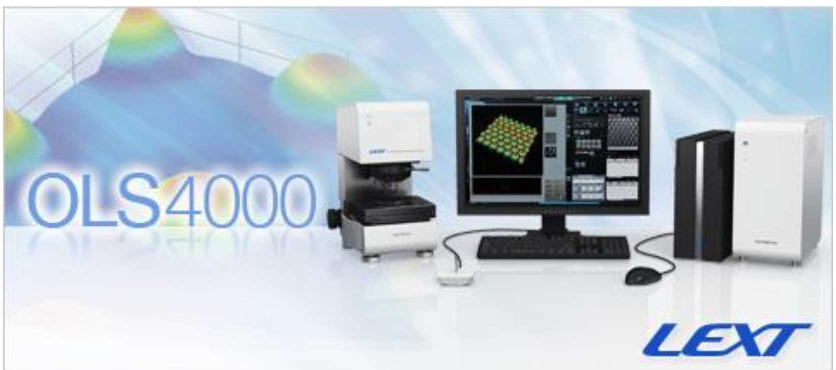

Figure 27 Optical microscope (Olympus laser microscopes model OLS 4000).

The fracture surface was then subjected to more detailed macroscopic and microscopic examinations using optical microscopes under ASTM E407. The procedures for preparing metallographic samples are as follows:

1. Metal sample prepared by selecting and cutting from the fracture surface of the specimen.

2. The sample of the fracture surface of the specimen was ultrasonically cleaned.

3. Mounting the sample in a synthetic resin cast into a small mold as follow in a Figure 28.

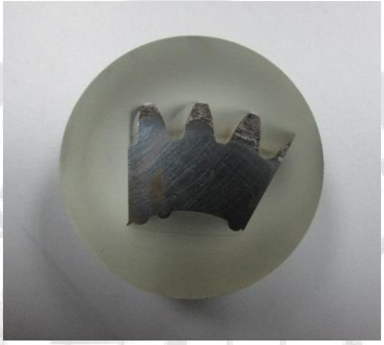

Figure 28 Mounting small a sample specimens in a synthetic resin.

4. Preliminary grinding of the embedded sample.

5. Polishing, Figure 29 shown using rotary discs impregnated with alumina or diamond powders on wet silicon carbide papers: usually papers of 400-1200 grit are employed.

Figure 29 Polishing of the specimen with rotary discs.

6. Examining the polished section with a metallurgical microscope.

7. Etching with 2 % Nital a suitable etching solution.

9. Doing photomicrography and drawings, if required, of the section to show microstructural details. In this case were look through a telescope 2 point at the outer surface and the central region as follows in Figure 30.

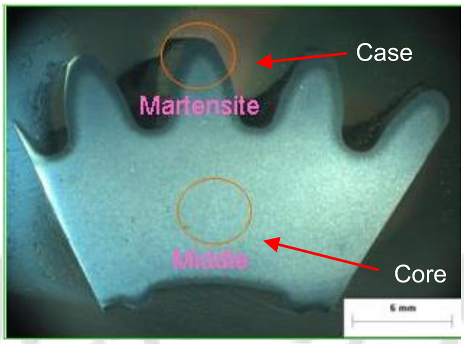

Figure 30 A sample specimen look through an optical microscopes at the outer surface and the central region.

The fracture surface was then subjected to more detailed microscopic examinations and inclusions were analyzed Energy Dispersive Spectroscopy (EDS) technique were using scanning electron microscopes (Hitachi model S-3400N) as show in a Figure 31, scanning electron microscope in order to look more closely at the nature of the fracture, Salient features of the fracture and respective photographs taken.

Figure 31 Scanning electron microscope (Hitachi model S-3400N).

The specimen must meet the following requirements before it is loaded to the SEM stage. The procedures for preparing metallographic samples were studied in the same manner optical microscope. Actual methods are as follows.

1. Grinding.

A small piece of specimen is cut by a metal-cutting-saw as follow in a Figure 32 After cutting operation, burrs on the edges of the specimen should be carefully removed by a fine file or coarse grinding paper.

Figure 32 A sample specimen of the fracture surface cutting from the pinion gear.

The silicon carbide grinding papers are held flat in a unit containing water facility for lubrication purpose. Each unit contains four grades of papers, starting with grade 400 (coarse) and finishing with grade 1200 (fine). Grinding of the work piece is done by starting with the coarse papers and then continuing with the fine papers. In each stage, grinding is done by rubbing the specimen backwards and forwards on the grinding paper in one direction only, until the surface is completely ground, that is, until only grinding marks due to this particular paper can be seen to cover the whole surface.

The specimen is washed thoroughly to remove coarse silicon carbide particles before proceeding to a finer paper. The direction of grinding is changed from paper to paper, so that the removal of previous grinding marks is easily observed. The extra time spent on each paper should be increased as the finer papers are used. At the end of the grinding sequence, the specimen is washed thoroughly and dried. Now, the specimen is ready for polishing.

2. Polishing.

The polishing is done on rotating wheels covered by a special cloth. Alumina is employed as polishing agent. The 1-micron size is commonly used, but the total polishing time shortened by starting on the 7 or 3 micron grade. The pad should be kept well supplied with lubricant. The specimen should be held firmly in contact with the polishing wheel, but excessive pressure should be avoided. During polishing the specimen should be rotated or moved around the wheel so as to give an even polish. The specimen should be thoroughly cleaned and dried between each wheel.

3. Etching.

Before etching, it is essential to ensure that the polished surface is grease and smear free. If the final polishing has involved the use of magnesia (in the form of an aqueous paste of fine magnesia) or alumina (in the form of an aqueous suspension of fine alumina), then thorough washing followed by drying off with acetone or alcohol will give a suitable surface, although it must not be fingered afterwards.

Etching is generally done by swabbing. Etching times will vary from specimen to specimen, however, a good general, procedure is to observe the surface during etching, and to remove the specimen when evidence of the grains first appears. Microscopical examination will then reveal whether the degree of etching is sufficient. Further etching can then follow to strengthen up the details as required.

After each etching, the specimen should be thoroughly washed in running water, followed by drying off with acetone or alcohol.

As a guide the following etchants are commonly used Nital (ethyl alcohol+ 2% HN03) -iron and steel.

4. Bring sample specimen into the scanning electron microscope to study and analyze the microstructure as follow in a Figure 33.

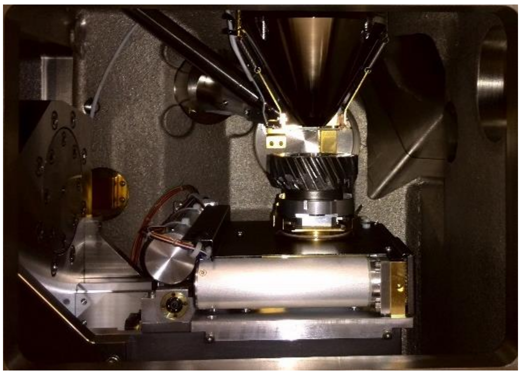

Figure 33 A sample specimen of the fracture surface into the scanning electron microscope.

5. The investigation result of the scanning electron microscopy is going to be recorded as follows:

- Examine each specimen and sketch typical microstructure
- Estimate the carbon content of the steels.

1.4 Bending and contact stresses analysis

Bending and contact stresses are calculated by using analytical method as well as finite element analysis. To estimate bending stress modified AGMA bending equation is used. Solid works 2014 modeling software is used to generate the 3-D solid model of the structural analysis of the helical gear tooth model is carried out using the finite element analysis and the boundary conditions were applied to the gear model. ANSYS 14.5 software package is used to analyze the bending stress. Contact stresses are calculated by using modified AGMA contact stress method. In this also Solid works 2014 modeling software is used to generate contact gear tooth model. ANSYS 14.5 software package is used to analyze the contact stress. Finally these two methods bending and contact stress results are compared with each other.

CHAPTER 4

RESULTS AND DISCUSSIONS

1. Chemical composition analysis

Chemical composition of the gear material was analysed using a spectrophotometer (THERMO: ARL 3460). The average values of the chemical composition of gear material are shown in Table 8. The compositions indicate that the gear was made from low-alloyed steels JIS G4053: Standard grade SCr 420, commonly and widely used in making gears. This means that proper material was used for making the gear. The details are obtained in Appendix B.

Table 8 Chemical composition of the failed gear and those of SCr 420 steel (%wt)

Material	Failed gear (Case)	Failed gear (Core)	SCr 420
C	0.564	0.223	0.18-0.23
Si	0.246	0.250	0.15-0.35
Mn	0.856	0.835	0.60-0.90
P	0.019	0.020	≤0.030
S	0.013	0.017	≤0.030
Ni	0.019	0.026	≤0.250
Cr	1.021	1.116	0.90-1.20

2. Visual examination

Visual examination of the failed helical gear showed that a number of adjacent teeth and random teeth failed by fatigue, as shown in Figure 34. Typical macro-fracture appearance of the failed helical gear tooth is shown in Figure 35 and Figure 36. The fracture surface presents typical features of fatigue failure. Similar fracture appearance was also observed on the other fracture surface of the gear teeth. A triangular piece of the gear teeth had broken off like a large chip at one end of the teeth. The pieces are as wide as one-third of the face width.

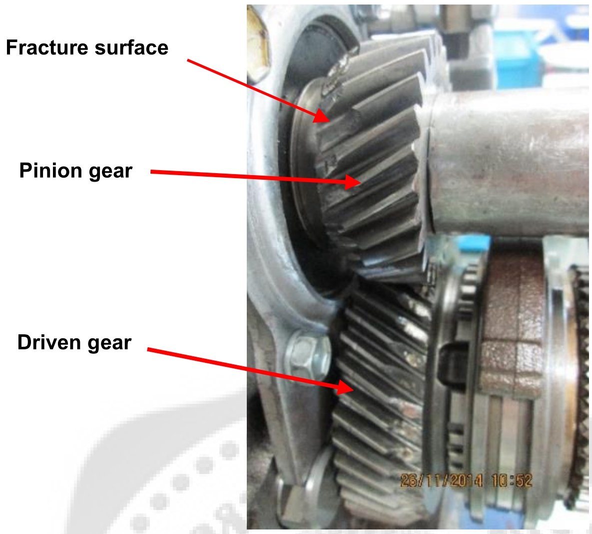

Figure 34 General appearance of the failed helical gear.

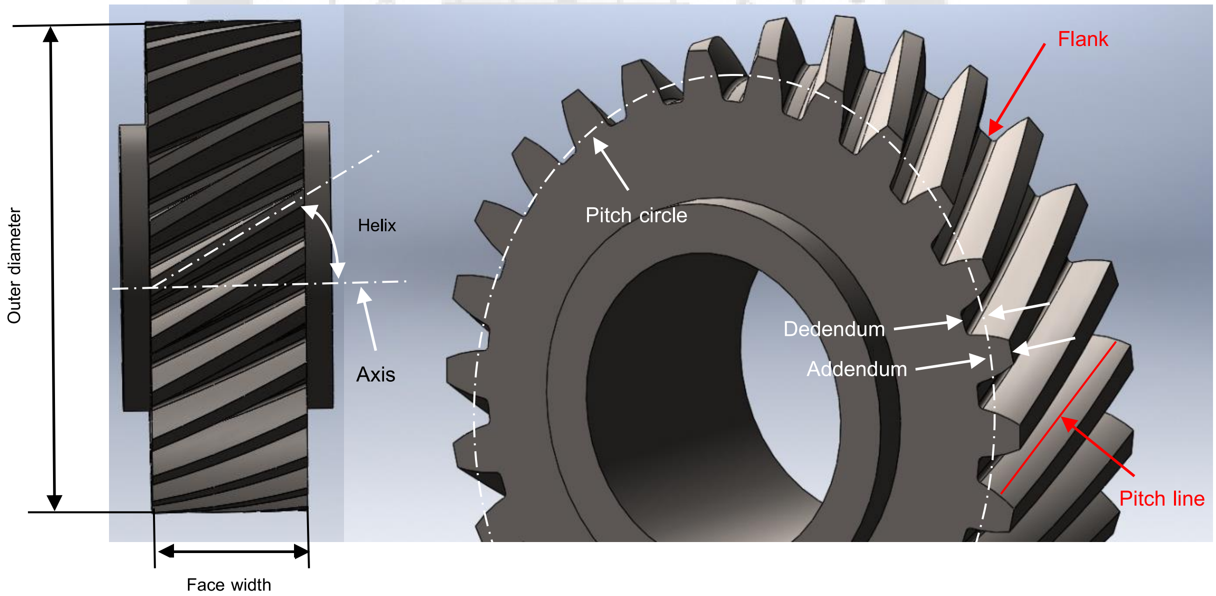

Figure 35 Nomenclature of the helical gear teeth.

The fracture of the tooth exhibits a distinct crack initiation site (indicated white arrow) and progressive flat fatigue fracture region, and the final fracture region. The crack initiation region and beach marks could be seen clearly with the naked eye. The origin of the crack was at the pitch line region close to one end of the gear teeth (indicated yellow arrow), suggesting that the loads were highest in this region.

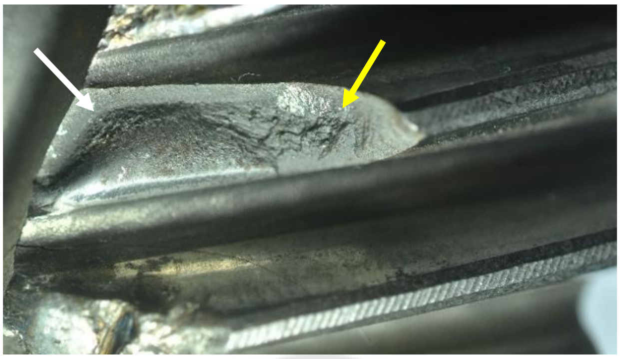

Figure 36 High magnification photograph of the fracture surface of the failed gear tooth**.**

3. Hardness measurements

The hardness distribution across the gear tooth thickness at the pitch line was measured using a micro Vickers hardness testing machines (Mitutoyo model HM-210A) with 300 gm load. The results are shown in Figure 36. The maximum hardness at the case and minimum at the core were found to be 780 HV (63.3 HRC) and 310 HV (31 HRC), respectively. Figure 37 indicated that the gear had been case hardened by carburization which is normal practice for gear heat treatment. The details are obtained in Appendix B.

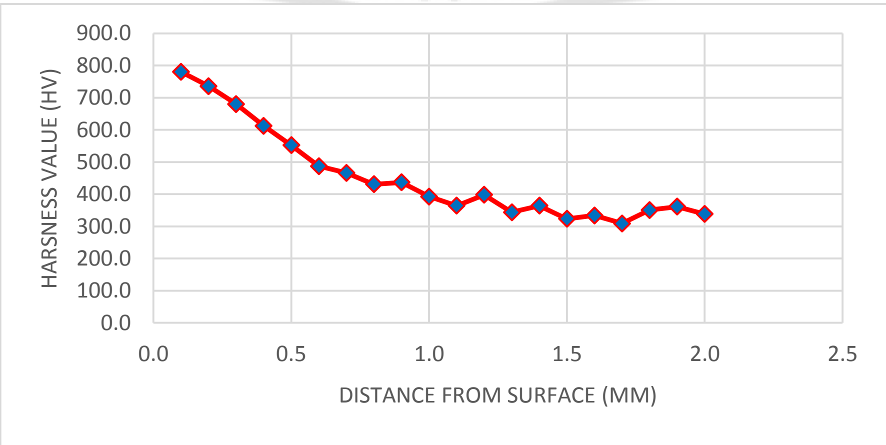

Figure 37 Hardness distribution across the failed gear tooth thickness at the pitch line.

4. Microstructure examination

Specimens from the failed gear tooth were metallographically prepared and examined under an optical microscope (OLYMPUS LASER MICROSCOPES: OLS 4000). The case microstructure is tempered martensite as shown in Figure 38a. The core is a mixture of ferrite and pearlite as shown in Figure 38b. The microstructure indicated that the gear heat treatment condition was carburized, quenched, and tempered which is common practice in heat treatment of SCr 420 steel. No abnormality was found in the microstructure.

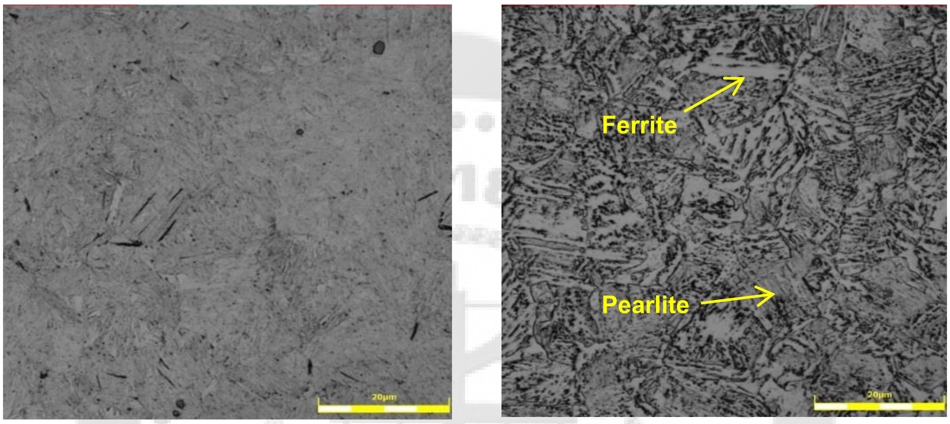

(a) (b)

Figure 38 Optical micrographs of the failed gear is showing (a) Case (tempered martensite). 4045x. (20 µm), (b) Core (mixture of pearlite + ferrite). 4045x. (20 µm)

The crack of the surface layer and examined under a scanning electron microscope (HITACHI: S-3400N). The failed gear outer surface region as show in Figure 39 can be seen as a transgranular fracture, This is a result of changes in orientation to the cleavage planes from grain to grain and intergranular fracture crack propagation along grain boundaries. These results indicate that the mode of fracture within this outer periphery of the gear was brittle. An SEM micrograph taken of the rough central region as shown in Figure 40, revealed the presence of both brittle cleavage features and also dimples; thus, it is apparent that the failure mode in this central interior region was mixed; that is, it was a combination of both brittle and ductile fractures.

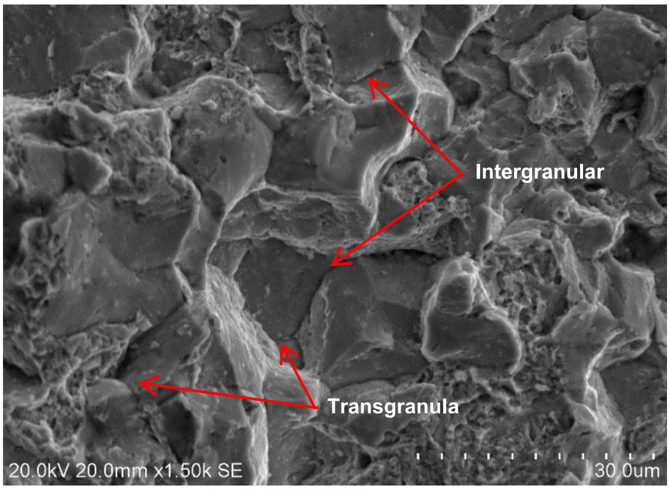

Figure 39 SEM micrograph showing the failed gear outer surface region, which is composed of mixed intergranular and transgranular regions. 1500x (30 μm)

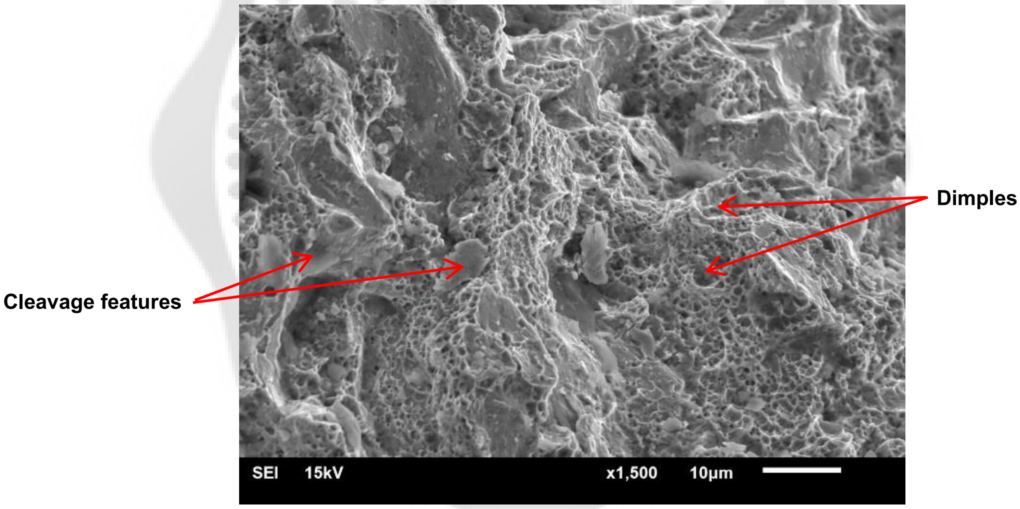

Figure 40 SEM micrograph showing the final overload fracture of the failed gear surface core region, which is composed of mixed cleavage and dimpled regions. 1500x (10 μm)

The crack in the surface layer at area 12 is shown in Figure 41 (a), when expanded at a ratio of 200x (200 μm) in Figure 41 (b), the EDS spectra of a scan can be seen that most of the Fe, C, and O is an important component. The elemental higher Si content in the inclusion than in the matrix at the area around the white circle. Considering Figure 42, respectively. Other elements present in the inclusion spectrum are O, Al, Mg and Na. The result suggested that the inclusion is a mixture of oxide and carbide. From the size, shape, and color of the inclusion, and the microanalysis result, it can be inferred that the inclusion is iron oxide surrounded by Fe_3C carbide.

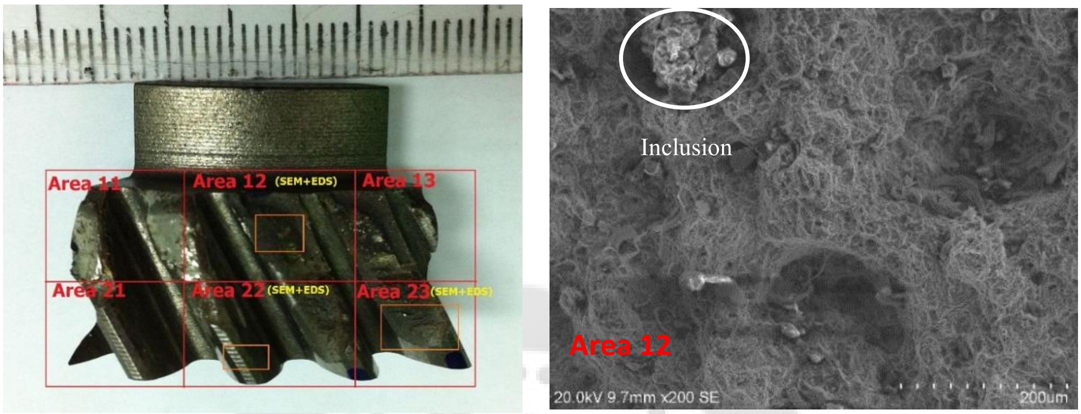

(a) (b)

Figure 41 High magnification photograph of failure gear is shown as (a) Crack of the core region at the area 12. (b) SEM and EDS micrograph of inclusions on the fracture surface from the area 12. 200x (200 μm).

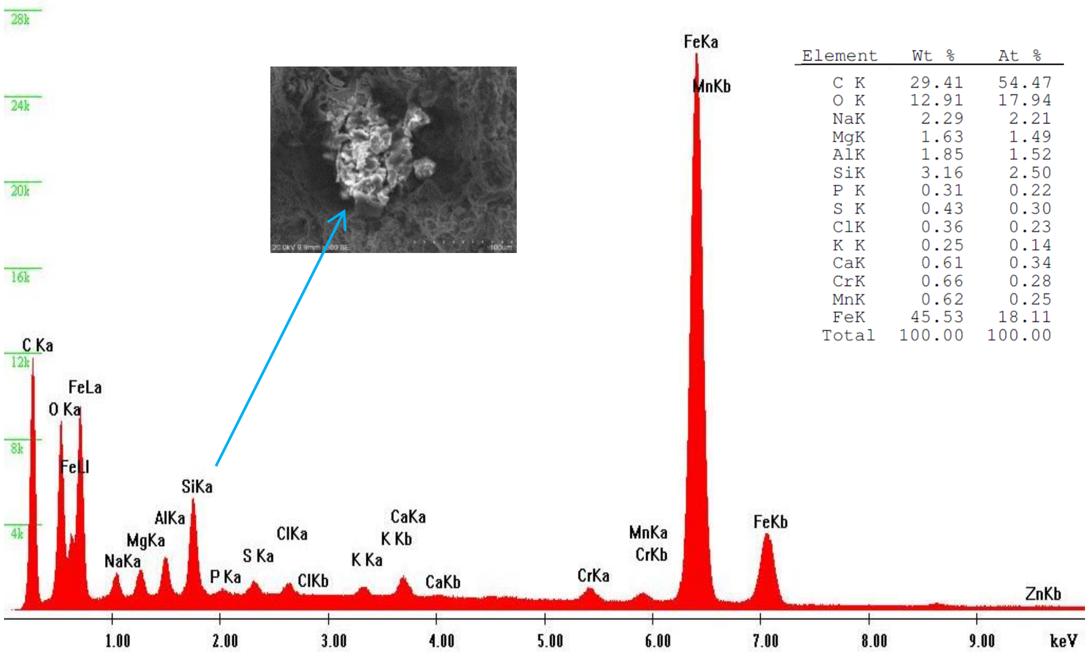

Figure 42 The EDS analysis diagram of inclusion indicated in the white circle area.

5. Bending equation

Parametric of helical gears let the characteristic parameters of a product. The main parameter that would describe the helical gear such as module, pressure angle and tooth thickness could be used as the parameters to define the gear as shown in Table 9.

Table 9 Dimensions of helical gear

Description	Symbol	Values	Unit
Power	H	120	kW
Speed	n_p	3200	rpm
Number of teeth pinion gear	N_p	26	-
Number of teeth drive gear	N_G	46	-
Pinion gear diameter	d_p	64	mm
Drive gear diameter	d_G	109	mm
Normal module	m	2.25	mm
Pressure angle	ϕ	30^{o}	degree
Helix angle	ψ	20^{o}	degree
Pitch diameter	d	103.5	mm
Pitch	P	58.5	mm
Gear face width	b	23	mm
Elastic coefficient	Z_E	191	N/mm^2

The AGMA equation for bending stresses given by,

$$\sigma_b = \frac{W^t K_o K_v K_s K_H K_B}{b m_t Y_J} \qquad (2\text{-}2)$$

Where,

The transverse metric module (m_t) = $\frac{m_n}{\cos\psi}$ = $\frac{2.25}{\cos 30^{\circ}}$ = 2.60 mm

Pitch-line velocity (V) = $\frac{\pi m_t N_p n_P}{60\times10^3}$ = $\frac{\pi\times2.6\times26\times3200}{60\times1000}$ = 11.32 m/s

Tangential transmitted load (W^t) $= \frac{H}{V} = \frac{120}{11.32}$ = 10.60 kN

Overload factor (K_o) = 1.25 Table 4

The size factor (K_s) = 1 Table 5

The load distribution factor K_H is determined from Eq. (2-3), where five terms are needed. They are, where b = 23 mm. in when needed:

$$(K_H) = 1 + C_{mc}(C_{pf}C_{pm} + C_{ma}C_e)$$

Uncrowned: C_{mc} = 1 Eq.2-4

The transverse diametral pitch (P_d) = $\frac{Z}{D\cos\psi} = \frac{26}{64\times\cos 30^{\circ}}$ = 0.47

Pitch diameter pinion gear (d_p) = $\frac{N_P}{P_d} = \frac{26}{0.47}$ = 55.32 mm

$C_{pf} = \frac{F}{10d_p} - 0.025 = \frac{23}{10\times 55.32} - 0.025$ = 0.016 Eq.2-5

Bearings immediately adjacent C_{pm} = 1 Eq.2-6

Commercial enclosed gear C_{ma} = 0.14 Fig 2.13

Mesh alignment correction factor C_e = 1 Eq.2-8

Thus,

K_H = 1 + $1[(0.016\times 1) + (0.14\times 1)]$ = 1.16

Dynamic factor (K_v) = $\left[\frac{59.77 + \sqrt{200\times 11.32}}{59.77}\right]^{0.8255}$ = 1.62 Eq.2-9

The rim-thickness factor (K_B) = 1 Table 2.6

Geometry factor for bending strength (Y_J) = 0.48 Fig 14, 15

$$\sigma_b = \frac{10.60\times 10^3\times 1.25\times 1.62\times 1\times 1.16\times 1}{23\times 2.60\times 0.48} = 867.45 \text{ N/mm}^2$$

5.1 Analysis bending stress using finite element method.

The structural analysis of the helical gear tooth model is carried out using the finite element analysis in Ansys 14.5. The load applied at the tooth of the helical gear. The mesh is generated with tetrahedral elements. Figure 43, shows the generated mesh. Maximum elements 41327 and maximum nodes 72325 were selected for the mesh control. By applying the analysis over the tooth which is facing the load we get the stress distribution in numerical.

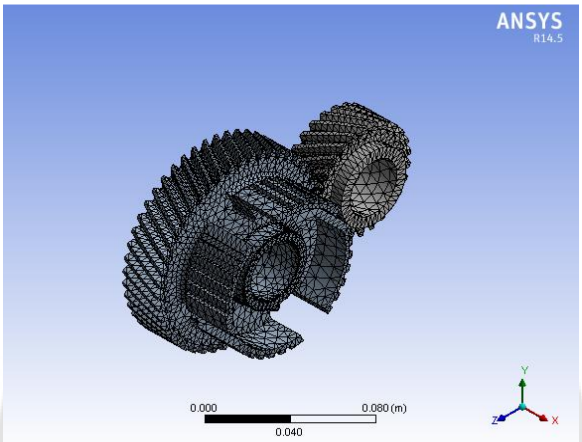

Figure 43 Meshed of helical gear model.

Finite element method results for bending, the helical gear assembly was imported in Ansys 14.5 and the boundary conditions were applied to the gear model. In helical gear only Ansys 14.5 analysis was performed because of the helical profile of its teeth. In Figure 44, it shows the stress distribution plot along the tooth from minimum to maximum of tangential transmitted load is 10.60 kN.

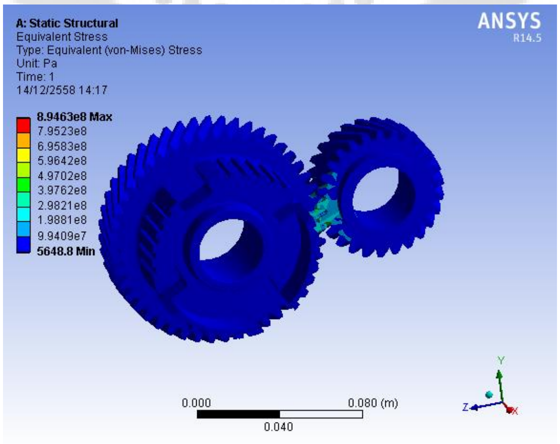

Figure 44 Von Mises stress (bending stresses of W^t 10.60 kN).

Effect of face width on maximum bending stress is studied by varying the face width (b = 23 mm) and helix angles (ψ = 30°). The maximum bending stresses obtained are shown in Table 10, there is a variation in the maximum bending stresses with the change from tangential transmitted load.

Table 10 Comparison of values of the bending stresses.

Torque (N.m)	**Tangential transmitted load W^t (kN)**	**Bending Stress σ_b AGMA (MPa)**	**Von Mises σ_b ANSYS (MPa)**
340	10.60	867.45	894.63
375	11.64	964.32	1048.41
405	12.56	1068.32	1132.38
430	13.38	1128.75	1202.24
455	14.12	1205.44	1272.16
475	14.80	1278.45	1328.62
490	15.41	1338.93	1369.93
515	15.97	1403.72	1439.87
535	16.48	1456.87	1495.75
545	16.96	1516.44	1523.76

The maximum bending stresses obtained are shown in Figure 45, it is evident in these that the bending stress given by AGMA and the finite element are very similar. The bending stress value increased with the increase of torque which is in close agreement with values obtained in the AGMA formula. The low alloy steel SCr 420 has the tensile strength of 1300 MPa.

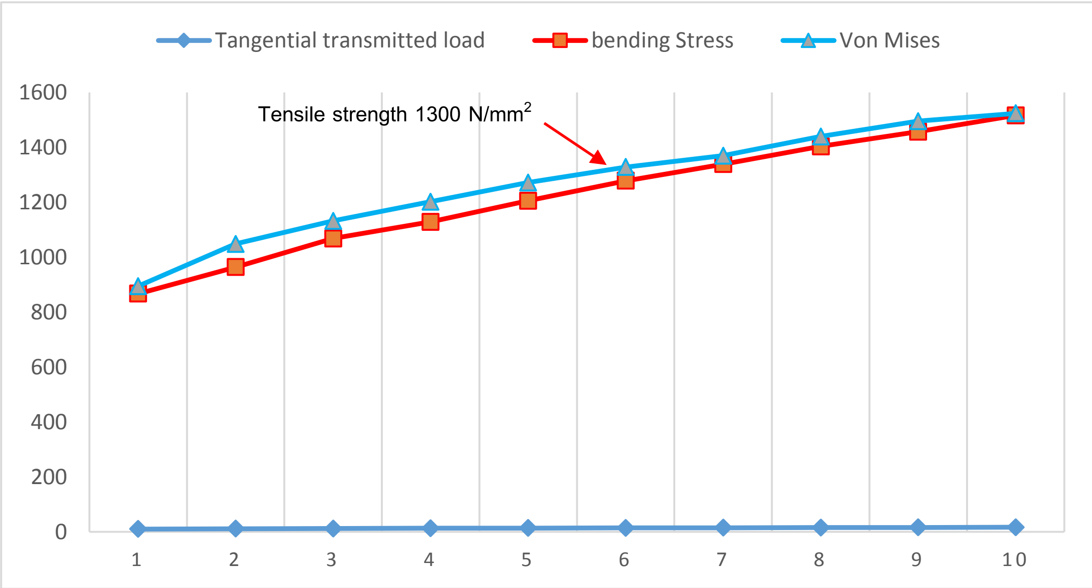

Figure 45 Graph between AGMA bending stress and Ansys results.

6. Contact stress

AGMA Contact Stress Equations

The fundamental equation for pitting resistance (contact stress) is

$$\sigma_c = Z_E \sqrt{\frac{W^t K_o K_v K_s K_H Z_R}{d_{w1} b Z_I}} \qquad (2\text{-}4)$$

Where,

Elastic coefficient (Z_E) = 191 $\sqrt{N/mm^2}$ Table 7

Tangential transmitted load (W^t) = $\frac{H}{V} = \frac{120}{11.32}$ = 10.60 kN

Overload factor (K_o) = 1.25 Table 4

The size factor (K_s) = 1 Table 5

The load distribution factor (K_H) = 1.16 Eq. 2-3

Dynamic factor (K_v) = $\left[\frac{59.77+\sqrt{200\times 11.32}}{59.77}\right]^{0.8255}$ = 1.62 Eq. 2-9

Surface condition factor (Z_R) = 1 Table 6

The pitch diameter of the pinion (d_{wl}) = = $N_p m_t$ = 26×2.60 = 67.60 mm.

Geometry factor of pitting resistance (Z_I) for helical gears requires a little work. First, the transverse pressure angle is given by

$$\phi_t = \tan^{-1}\left(\frac{\tan\phi_n}{\cos\psi}\right) = \tan^{-1}\left(\frac{\tan 20^\circ}{\cos 30^\circ}\right) = 22.80^\circ$$

where the pinion base-circle radius $(r_b)_p$ and $(r_b)_G$ the gear base-circle radius from Eq.2-16

$$(r_b)_p = r_p \cos\phi_t = 32 \times \cos 22.80^\circ = 29.50 \text{ mm}$$

$$(r_b)_G = r_G \cos\phi_t = 54.5 \times \cos 22.80^\circ = 50.24 \text{ mm}$$

The speed ratio $m_G = \dfrac{N_G}{N_P} = \dfrac{46}{26}$ = 1.77 Eq.2-12

$$P_n = \pi m_n = \pi \times 2.25 = 7.07$$

Addendum $a = \dfrac{1}{P_n} = \dfrac{1}{7.07}$ = 0.14

$$Z = \left[(r_p + a)^2 - {r_{bP}}^2\right]^{\frac{1}{2}} + \left[(r_G + a)^2 - {r_{bG}}^2\right]^{\frac{1}{2}} - (r_P + r_G)\sin\phi_t \qquad \text{Eq.2-15}$$

$$Z = \sqrt{(32+0.14)^2 - 29.50^2} + \sqrt{(54.5+0.14)^2 - 50.24^2} - (32+54.5)\sin 22.80^\circ$$

Z = 12.76 + 21.48 – 33.52 = 0.72

The normal circular pitch $P_N = P_n \cos\phi_n = \dfrac{\pi}{P_n}\cos 20^\circ$

$$= \frac{\pi}{7.07}\cos 20^\circ = 0.42 \qquad \text{Eq.2-14}$$

The load-sharing ratio $m_N = \dfrac{P_N}{0.95Z} = \dfrac{0.42}{0.95 \times 0.72}$ = 0.61 Eq.2-11

Geometry factor $Z_I = \dfrac{\cos\phi_t \sin\phi_t}{2m_N}\dfrac{m_G}{m_G + 1}$

$$= \frac{\cos 22.80 \sin 22.80}{2 \times 0.61}\frac{1.77}{1.77+1} = 0.19 \qquad \text{Eq.2-13}$$

$$\sigma_c = 191\sqrt{\frac{10.60 \times 10^3 \times 1.25 \times 1.62 \times 1 \times 1.16 \times 1}{67.55 \times 23 \times 0.19}} = 1753.53 \text{ N/mm}^2$$

6.1 Analysis contact stress using finite element method.

Contact stresses were studied in the same manner as bending stresses were calculated. In this research contact stresses are obtained at the contact region. The Figure 46 shows the stress distribution plot along the tooth. The modeled helical gear is analyzed to study the effect of tangential transmitted load (W^t). The minimum to maximum contact stresses obtained are shown in Table 11, there is a variation in the maximum contact stresses with the change from tangential transmitted load.

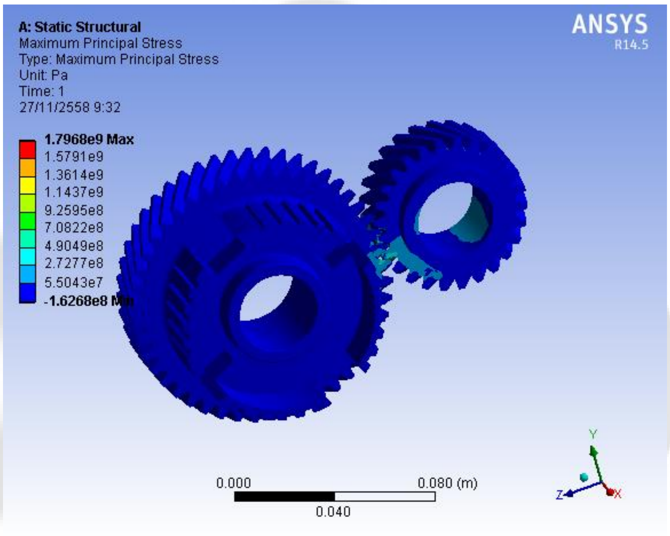

Figure 46 Maximum principal stress (Contact stresses of W_t 10.60 kN).

The maximum contact stresses obtained are shown in Figure 47, it can be seen the contact stress given by AGMA and the finite element are very similar. Stress starts from contact stress on the surface of a gear tooth and bending stress is then extended to the central axis of the gear which is the contact stress as a result of final fracture when the torque is higher than the tensile strength of 1300 MPa. The conclusion is that if the torque exceeds the tensile strength to accept it as a reason for the split while the gear shifts.

Table 11 Comparison of values of the contact stresses.

Torque (N.m)	Tangential transmitted load W^t (kN)	Contact Stress σ_c AGMA (MPa)	Principal Stress σ_c ANSYS (MPa)
80	2.56	834.73	955.76
150	4.71	1139.66	1198.12
210	6.52	1349.55	1395.85
260	8.07	1511.01	1578.23
305	9.42	1642.82	1718.30
340	10.60	1753.53	1796.80
375	11.64	1848.85	1908.47
405	12.56	1932.20	1977.54
430	13.38	2000.27	2089.65
455	14.12	2067.11	2178.91

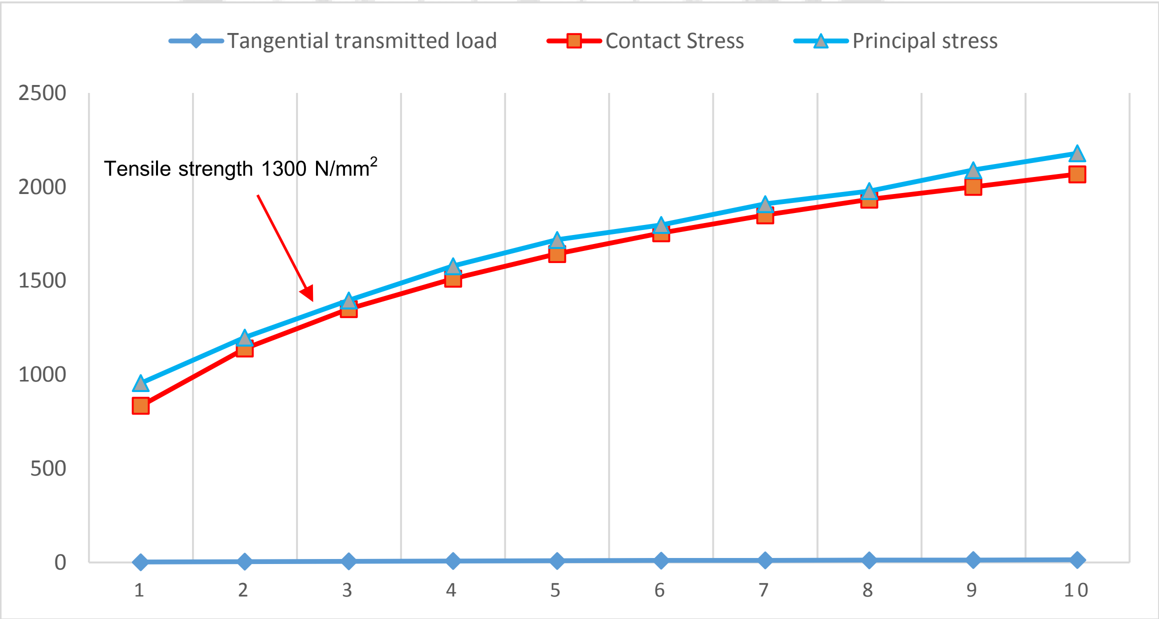

Figure 47 Graph between AGMA contact stress and Ansys results.

CHAPTER 5

CONCLUSION AND SUGGESTION

1. Conclusion

This study was conducted on a failed helical gear used in a pick-up car. The composition (wt%) analysis, mechanical property and microstructure analysis of the failed gear was made from JIS-SCr 420 steel in it hardened and tempered condition can be summarized as follows.

The crack of the outer surface region can be seen as a transgranular fracture and intergranular fracture which these results indicate the mode of the fracture within this outer periphery of the gear in which it was brittle and microstructure is tempered martensite. The central region revealed the presence of both brittle cleavage features and also dimples which it was a combination of both brittle and a ductile fracture, the microstructure is a mixture of ferrite and pearlite.

The failure was due to fatigue, any increase in the loading level of this core region would have occurred relatively slowly. During the gradually increasing load level, fatigue crack propagation would have continued until a critical length was achieved the remaining intact gear's cross section was no longer capable of sustaining the applied load. At this time, final failure would have occurred in the gear fracture.

The total percentage of oxides and carbides in the microstructure to be the cause of the damage occurred in the gear tooth. In this case the mixing failure area of oxide inclusion with carbide surrounding before the liquid state of material will be solidified which is difficult to control in manufacturing. It is recommended that cleaner steels be used to make such high reliability gears which could be achieved via improved steel making practice.

Stress starts from contact stress on the surface of a gear tooth and bending stress is then extended to the central axis of the gear which is the contact stress as a result of final fracture when the torque is higher than tensile strength of material 1300 N/mm^2, which will benefit the gear design. (In such cases, it will allow the car to increase engine power and see the damage when it occurs. Because it affects to the transmission and differential.)

2. Suggestion

The following areas are worthy for further research in the light of this work.

1. The study of failure gear tooth mechanisms of oil film on the gear contact zone.

2. The study of failed mechanisms on gears are a continuously evolving field of research. As the gear geometries, manufacturing methods materials, new failures can emerge.

3. Finite element methods of investigation and study can be conducted on the whole gearbox with all elements in the system including gear casing such as shaft and bearing.

4. Finite element methods of investigation and study can be conducted on the analysis of bending and contact stresses for all types of gears such as a spur gear, bevel and worm gears.

REFERENCES

REFERENCES

David A. Scott. (1991). *Metallography and microstructure of ancient and historic metals*. Singapore: Tien Wah Press, Ltd.

Sidney H. Arner. (1997). *Introduction to Physical Metallurgy*. New York: McGraw-Hill.

JIS G 4053. (2003). *Japanese Industrial Standard*. Tokyo: Japan.

Sermsak Kateboonlue. (2004). *Analysis of the Stress Distribution in Spur and Helical Gear Teeth by the Finite Element Method*. Master of Engineering. Mechanical Engineering Division. Faculty of Engineering. Kasetsart University. Photocopied.

Anat Hasap. (2005). *Wear characteristics of miniature spur gear in high precision transmission systems. Master of Engineering*. Mechanical Engineering Division. Faculty of Engineering. King Mongkut's Institute of Technology Ladkrabang. Photocopied.

Osman Asi. (2005). *Fatigue Failure of a Helical Gear in a Gearbox*. Engineering Failure Analysis. 13(7): 1116-1125.

William D. Callister, Jr. (2005). *Materials Science and Engineering an Introduction*. Bangkok: Top Publishing Co., Ltd.

Daryl L. Logan. (2007). *A first course in the finite element method*. Toronto: Thomson Canada Limited.

C. Kendall Clarke and Don Halimunanda. (2008). *Failure Analysis of Induction Hardened Automotive Axles*. Journal of Failure Analysis and Prevention. 8(4): 386-396

Samroeng Netpu; & Panya Srichandr. (2012). *Failure Analysis of a Helical Gear in a Gearbox Used in a Steel Rolling Mill*. Journal of Materials Science and Engineering. 2(4): 289-294.

Charnont Moolwan; & Samroeng Netpu. (2012). *Failure analysis of a two high gearbox shaft*. Engineering and Energy Conference 2012. 88: 154-163.

Govind T Sarkar; Yogesh L Yenarkar; & Dipak V Bhope. (2013). *Stress analysis of helical gear by finite element method*. International Journal of Mechanical Engineering and Robotics Research. 2: 323-329.

J. Venkatesh; & Mr. P. B. G. S. N. Murthy. (2014). *Design and Structural Analysis of High Speed Helical Gear Using Ansys*. J. Venkatesh Int. Journal of Engineering Research and Applications. 4(3): 1-5.

Sandeep S Kadam; & Prof. S. D. Ambekar. (2014). *Dry Sliding Wear Behavior Of Carburized 20mncr5 Alloy Steel*. International Journal of Engineering Science Invention. 3(5): 67-72.

Joseph Edward Shigley. (2015). *Mechanical Engineering Design*. New York: McGraw-Hill.

Material special sheet. Retrieved April 18, 2015, from http://www.saarstahl.com/fileadmin/saarstahl_extranet/images/04_produkte/walzstahsorten/english/7147_7149_20MnCr_20MnCS5.pdf.

APPENDIX

APPENDIX A

List of symbols

LIST OF SYMBOLS

Symbol		Description	Unit
b	=	Gear face width	mm
C	=	Carbon	%wt
C_e	=	Mesh alignment correction factor	-
C_{ma}	=	Mesh alignment factor	-
C_{mc}	=	Load correction factor	-
C_{pf}	=	Pinion proportion factor	-
C_{pm}	=	Bearings immediately adjacent	-
Cr	=	Chromium	%wt
d	=	Pitch diameter	mm
d_G	=	Pitch diameter drive gear	mm
d_p	=	Pitch diameter pinion gear	mm
d_{wl}	=	Pitch diameter of the pinion	mm
H	=	Power	kW
J'	=	Helical-gear geometry factors	-
K_B	=	Thickness Factor	-
K_f	=	Fatigue stress-concentration factor	-
K_H	=	Load-Distribution Factor	-
K_o	=	Overload Factor	-
K_R	=	Rim-thickness factor	-
K_s	=	Size Factor	-
K_v	=	Dynamic factor	-
m	=	Normal module	m
m_F	=	Face-contact ratio	-
m_n	=	Normal module	m
m_N	=	Load-sharing ratio	-

LIST OF SYMBOLS (continued)

Symbol		Description	Unit
Mn	=	Manganese	%wt
m_P	=	Transverse contact ratio	-
m_t	=	Transverse metric module	mm
Ni	=	Nickel	%wt
n_p	=	Speed	rpm
N_G	=	Number of teeth drive gear	-
N_p	=	Number of teeth pinion gear	-
P	=	Phosphorus	%wt
P_d	=	Transverse diametral pitch	mm
P_N	=	Normal base pitch	mm
Q_v	=	Quality numbers	-
r_G	=	Pitch-circle radius, gear	mm
r_P	=	Pitch-circle radius, pinion	mm
r_{bP}	=	Pinion base-circle radius	mm
r_{bG}	=	Gear base-circle radius	mm
S	=	Sulfur	%wt
Si	=	Silicon	%wt
V	=	Pitch-line velocity	m/s
W^t	=	Tangential transmitted load	N
Y_J	=	Bending-Strength Geometry Factor	-
Z_I	=	Surface-Strength Geometry Factor	-
Z_E	=	The Elastic Coefficient	N/mm^2
x, y, z	=	structure global or reference coordinate axes	-
ϕ	=	Pressure angle	degree
ϕ_n	=	Normal pressure angle	degree

LIST OF SYMBOLS (continued)

Symbol		Description	Unit
ϕ_t	=	Transverse pressure angle	degree
ψ	=	Helix angle	degree
σ_b	=	Bending stress	N/mm^2
σ_c	=	Contact stress	N/mm^2
σ_x, σ_y, σ_z	=	Shear stresses act in the faces (planes) of the element	N/mm^2
τ	=	Normal strain	N.m
ε	=	Normal strain	-
ν	=	Poisson's ratio	-
α	=	coefficient of thermal expansion	-

APPENDIX B

Properties of selected engineering material

saarstahl

Material specification sheet

Saarstahl - 20MnCr5 - 20MnCrS5

Material No.:	Former brand name:	International steel grades:
1.7147	**EC 100**	**BS:**
		AFNOR: 20MC5
1.7149		**SAE:** 5120

Material group: Case hardening steels according to DIN EN 10084

Chemical composition: (Typical analysis in %)

Steel	C	Si	Mn	Cr	S	other
20MnCr5	0,20	0,25	1,25	1,15	<0,035	(Pb)
20MnCrS5	0,20	0,25	1,25	1,15	0,020 0,035	(Pb)

Application: Alloyed case hardening steel for parts with a required core tensile strength of 1000 - 1300 N/mm² and good wearing resistance as boxes, piston bolts, spindles, camshafts, gears, shafts and other mechanical controlling parts.

Hot forming and heat treatment:

Forging or hot rolling:	1100 - 850°C
Normalising:	840 - 870°C/air
Soft annealing:	650 - 700°C/furnace
Carburising:	880 - 980°C
Core hardening:	860 - 900°C/oil
Intermediate annealing:	650 - 700°C
Case hardening:	780 - 820°C/oil
Tempering:	150 - 200°C

Mechanical Properties:

Treated for cold shearability, +S:	max. 255 HB
Soft annealed, +A:	max. 217 HB
Treated for strength, +TH:	170 - 217 HB
Treated for ferrite and pearlite structure and hardness range, +FP:	152 - 201 HB

after hardening and tempering at 200°C:

Diameter d [mm]	d <= 16	16 <d <= 40	40 <d <= 100
Tensile strength R_m [N/mm²]	min. 1200	min. 1000	min. 800

LPN METALLURGICAL RESEARCH CENTER (THAILAND) CO., LTD.
299 Moo 2, Suksawad Road, Naikhlongbangplakot, Phra Samut Chedi, Samut Prakan 10290 Thailand
Tel. +66 2 815 4118-9, Fax. +66 2 815 4120, www.lpnmrc.com

Hardness Testing Report

Customer :S.H.K. ENGINEERING CO.,LTD

Address :70/4 Moo 3 suksawat 74 R., Bangkru, Phrapradang, Samutprakarn 10130 Thailand.

Report No. HV-15-05-001

Revision No. 0

Test Product	GEAR
Test No.	1162/15 HN
Test Location	N/A
Project Name / Project No.	N/A
Material Specification	18 Cr NiMo steel
Dimension	N/A
Welding Process/Position	N/A
Type of Joint / Weld	N/A
Welder Name / No.	N/A
Date Received	29 April 2015

Material Characterization	N/A
Test Method	ASTM E92-82 (Reapproved 2003)^{e2}
Standard of Test	N/A
Type of test	Vicker Hardness Test
Equipment	Wilson Wolpert , 432 SVD (V32D219)
Indentor Size	Pyramid diamond, angle of 136°
Test Load	HV 0.3 Kgf.
Total Force Dwell Time	15 s
Cal. Block	No. A60056 , No. 224 - 803
Ambient Temperature	25.5 °C
Date Tested	04 May 2015

Test Location
Total = 20 points

HV 0.3 Kgf

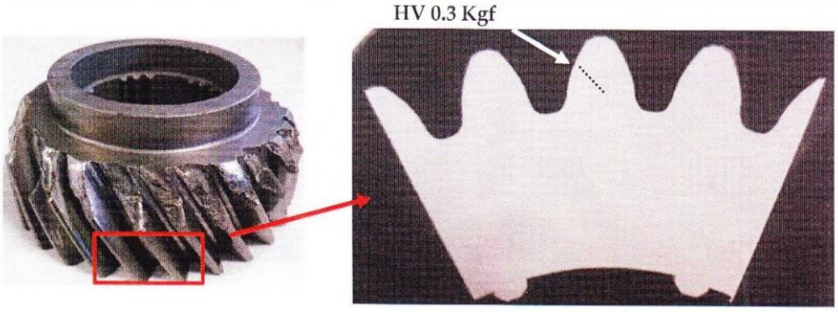

Point No.	Location	Hardness value (Scale HV)	Point No.	Location	Hardness value (Scale HV)	Point No.	Location	Hardness value (Scale)
1	BASE	780.4	16	BASE	333.4			
2	BASE	735.6	17	BASE	308.7			
3	BASE	680.1	18	BASE	350.4			
4	BASE	612.0	19	BASE	361.1			
5	BASE	551.9	20	BASE	338.3			
6	BASE	487.0	************************					
7	BASE	466.1						
8	BASE	430.5						
9	BASE	436.5						
10	BASE	392.5						
11	BASE	363.9						
12	BASE	397.7						
13	BASE	343.4						
14	BASE	363.9						
15	BASE	323.0						

Additional details : -

Reported by : Jantarat
(Miss. Jantarat Konggapee)
Metallurgical Analysis and Chemical Manager
Date : 05 / 05 / 15

Approved by : Pavaret
(Mr.Pavaret Preedawiphat)
Director
LPN METALLURGICAL RESEARCH CENTER
Date : 05 / 05 / 15

Notes
1. The above results are valid exclusively for tested samples as mentioned in this report.
2. Partial publicity of the results on testing is prohibited without the written permission from LPN MRC.
3. This report shall not be reproduced in whole or in part without the written approval of LPN MRC.

LPN METALLURGICAL RESEARCH CENTER (THAILAND) CO., LTD.
299 Moo 2, Suksawad Road, Naikhlongbangplakot, Phra Samut Chedi, Samut Prakan 10290 Thailand
Tel. +66 2 815 4118-9, Fax. +66 2 815 4120, www.lpnmrc.com

Hardness Testing Report

Customer :S.H.K. ENGINEERING CO.,LTD

Address :70/4 Moo 3 suksawat 74 R., Bangkru, Phrapradang, Samutprakarn 10130 Thailand.

Report No. HV-15-05-001

Revision No. 0

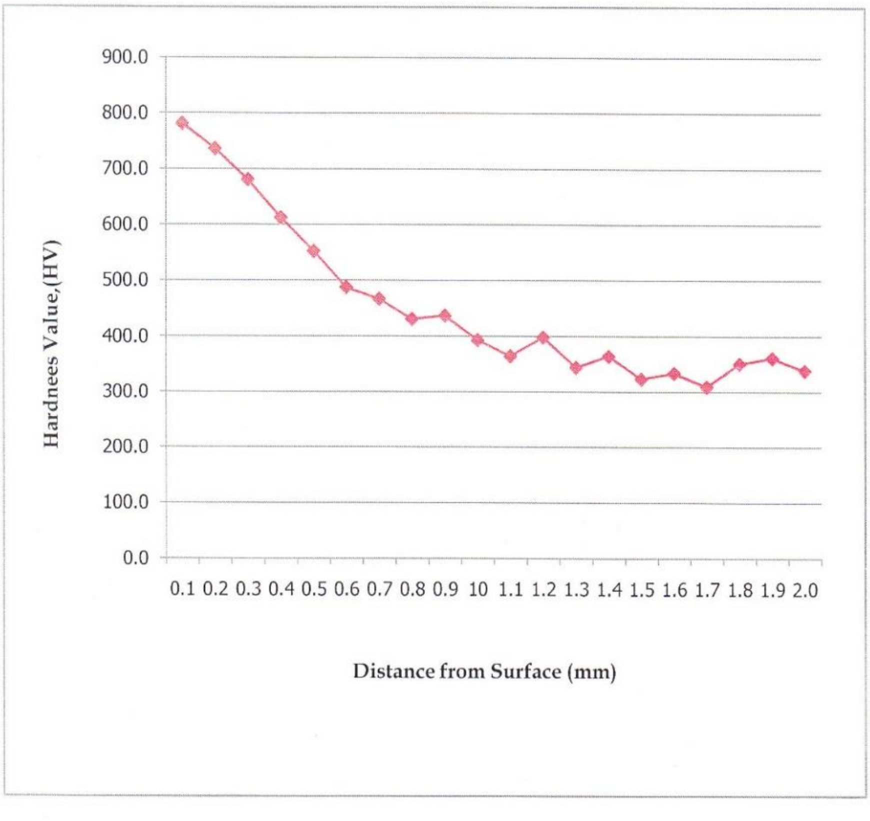

Additional details : -

Reported by : Jantarat
(Miss. Jantarat Konggapee)
Metallurgical Analysis and Chemical Manager
Date : 05/05/15

Approved by : ....
(Mr.Pavaret Pruedawiphat)
Director
LPN METALLURGICAL RESEARCH CENTER
Date : 05/05/15

Notes

1. The above results are valid exclusively for tested samples as mentioned in this report.
2. Partial publicity of the results on testing is prohibited without the written permission from LPN MRC.
3. This report shall not be reproduced in whole or in part without the written approval of LPN MRC.

APPENDIX C

Kasem Bundit engineering journal

วิศวกรรมสารเกษมบัณฑิต

ปีที่ 5 ฉบับที่ 2 กรกฎาคม - ธันวาคม 2558

Kasem Bundit Engineering Journal (KBEJ)

Volume 5 No.2 July - December 2015

คณะวิศวกรรมศาสตร์ มหาวิทยาลัยเกษมบัณฑิต

วิศวกรรมสารเกษมบัณฑิต
Kasem Bundit Engineering Journal (KBEJ)
คณะวิศวกรรมศาสตร์ มหาวิทยาลัยเกษมบัณฑิต

วิศวกรรมสารเกษมบัณฑิตจัดทำขึ้นเพื่อเผยแพร่ผลงานวิจัยและพัฒนา ผลงานวิชาการ ตลอดจนองค์ความรู้ทางด้านวิศวกรรมศาสตร์ของอาจารย์ นักวิชาการอิสระ และวิศวกรทั่วไป และเป็นสื่อกลางระหว่างมหาวิทยาลัยเกษมบัณฑิตกับสังคมภายนอกในการเผยแพร่ความรู้ต่าง ๆ ด้านวิศวกรรมศาสตร์ เพื่อให้เป็นฐานความรู้อันจะนำไปสู่การพัฒนาด้านวิศวกรรมต่อไป โดยมีกำหนดตีพิมพ์ปีละ 2 ฉบับ ออกเป็นราย 6 เดือน (ประจำเดือนมกราคม - มิถุนายน และ กรกฎาคม - ธันวาคม)

วัตถุประสงค์

- เพื่อเป็นเอกสารเผยแพร่งานวิจัยของคณะวิศวกรรมศาสตร์ มหาวิทยาลัยเกษมบัณฑิต
- เพื่อเป็นแหล่งเผยแพร่งานวิจัยและพัฒนา และผลงานวิชาการของคณาจารย์ทั้งในและนอกสถาบัน ตลอดจนนักวิชาการอิสระและวิศวกรทั่วไป
- เพื่อส่งเสริมและกระตุ้นให้เกิดการวิจัยทั้งภายในและภายนอกสถาบัน ส่งผลให้มีการต่อยอดงานวิจัยและการพัฒนาองค์ความรู้ทางวิศวกรรม เพื่อให้เกิดความเชื่อมโยงระหว่างวิชาการและวิชาชีพ อันจะเป็นประโยชน์แก่ชุมชนและสังคมโดยรวม
- เพื่อสร้างกลไกสนับสนุนการเผยแพร่รวมถึงระบบการรวบรวมและคัดสรรผลงานวิจัยและงานสร้างสรรค์เพื่อนำไปใช้ประโยชน์ทั้งในวงวิชาการและวิชาชีพ ซึ่งถือเป็นส่วนหนึ่งของการประกันคุณภาพการศึกษา

กำหนดตีพิมพ์

ปีละ 2 ฉบับ ออกเป็นราย 6 เดือน (ประจำเดือนมกราคม - มิถุนายน และ กรกฎาคม - ธันวาคม)

จัดพิมพ์โดย คณะวิศวกรรมศาสตร์ มหาวิทยาลัยเกษมบัณฑิต

บทบรรณาธิการ

ในวาระอันเป็นศุภฤกษ์ที่เวียนมาบรรจบครบรอบอีกวาระหนึ่ง ในนามกองบรรณาธิการขอถือโอกาสนี้กล่าวขอบพระคุณคณะกรรมการสภา ผู้บริหารมหาวิทยาลัยที่ให้การสนับสนุนด้านการเงินและกำลังใจ คณะผู้ทรงคุณวุฒิ คณะนักวิจัย และคณะทำงาน ที่สนับสนุน แรงสมอง แรงกายและแรงใจ ที่มีส่วนร่วมในการผลักดันให้วารสารฉบับนี้เติบโตมาอย่างต่อเนื่อง จนได้รับการประกาศให้เข้าสู่การเป็นฐานข้อมูลดัชนีการอ้างอิงวารสารไทย (Thai-Journal Citation Index) ในรอบปีที่ผ่านมา และขอถือโอกาสนี้อำนวยพรให้ท่านทั้งหลายได้ประสบแต่ความสุข ความเจริญ ทั้งในด้านหน้าที่การงานและสุขภาพร่างกายตลอดปี พ.ศ. 2559 นี้เทอญ

และในโอกาสนี้ กองบรรณาธิการขอแจ้งให้ท่านทั้งหลายได้รับทราบถึงแนวปณิธานที่แน่วแน่จะพัฒนาวารสารทางวิชาการฉบับนี้ ให้เป็นสื่อกลางทางด้านวิศวกรรมศาสตร์ ที่มีคุณภาพดียิ่ง ๆ ขึ้นไปและให้ได้รับการอ้างอิงทั้งในระดับชาติและนานาชาติต่อไป

รองศาสตราจารย์ ดร.ชัยฤทธิ์ สัตยาประเสริฐ
บรรณาธิการวิศวกรรมสารเกษมบัณฑิต

สารบัญ (ต่อ)

บทความวิจัย (ต่อ)

บทความทางวิชาการ

สมบัติทางกลและโครงสร้างจุลภาคของการวิเคราะห์ความเสียหายที่ส่งผ่านเฟืองเฉียงรถยนต์บรรทุกขนาดเล็ก

MECHANICAL PROPERTIES AND MICROSTRUCTURE OF PICKUP'S HELICAL GEAR TRANSMISSION FAILURE ANALYSES

วิษณุ บุญมาก และ กัณวริช พลูปราชญ์
ภาควิชาวิศวกรรมเครื่องกล, คณะวิศวกรรมศาสตร์ มหาวิทยาลัยศรีนครินทรวิโรฒ
ถ. รังสิต-นครนายก อ. องครักษ์ จ. นครนายก 26120

Visanu Boonmag[1] Ganwarich Pluphrach[1]
[1]Department of Mechanical Engineering, Faculty of Mechanical Engineering,
Srinakharinwirot University, Rangsit-Nakornnayok Rd., Ongkharak, Nakhornnayok 26120

บทคัดย่อ

การแตกหักของเฟืองเฉียงขับที่ตำแหน่งเกียร์ 5 ในรถปิ๊กอัพคันหนึ่งที่มีอายุการใช้งานมานานกว่า 6 ปี โดยมีการบำรุงรักษาอย่างถูกวิธี เฟืองทำจากเหล็กกล้าผสมต่ำ JIS-SCr 420 การวิเคราะห์ความเสียหายของเฟืองมีหลายวิธีคือ 1) การวิเคราะห์ส่วนผสมทางเคมีด้วยเครื่อง Spectrometer 2) การตรวจสอบความแข็งด้วยวิธีวิกเกอร์ส 3) การวิเคราะห์โครงสร้างจุลภาคด้วยกล้องจุลทรรศน์แบบใช้แสง สำหรับการตรวจสอบโครงสร้างจุลภาคและการวิเคราะห์ธาตุเชิงปริมาณ พิจารณาด้วยกล้องจุลทรรศน์อิเล็กตรอนแบบส่องกราด 4) การวิเคราะห์ความเค้นดัดของเฟืองด้วยสมการ AGMA และ 5) การเปรียบเทียบผลลัพธ์ทั้งหมดร่วมกับวิธีไฟไนต์เอลิเมนต์ ผลของการวิเคราะห์สรุปได้ว่า การแตกหักของเฟืองเฉียงขับเกิดจากความล้าซึ่งเป็นผลมาจากความเค้นดัดที่เกินค่า Tensile strength ของวัสดุ 1300 MPa ลักษณะรอยแตกบริเวณผิวรอบนอกของเฟืองมีการแตกผ่านเกรน และการแตกระหว่างเกรน ซึ่งเป็นการแตกหักแบบเปราะ ส่วนที่แกนกลางของเฟืองมีการแตกแบบแยกออกและแบบรอยบุ๋ม ความเสียหายในบริเวณนี้เป็นแบบผสมมีการแตกหักแบบเปราะและแบบเหนียวปนกัน โดยที่สามารถเห็นการรวมเป็นส่วนผสมของออกไซด์ล้อมรอบด้วยคาร์ไบด์ ก่อนที่จะมีการเปลี่ยนสถานะจากของเหลวเป็นของแข็ง ซึ่งเป็นเหตุแห่งความเสียหายที่เกิดขึ้นในฟันเฟืองเฉียงดังกล่าว ทั้งนี้ผลของการวิเคราะห์สอดคล้องกับสมมติฐานที่ได้กำหนดไว้พร้อมเป็นข้อมูลสำหรับการหาวิธีป้องกันมิให้เกิดการชำรุดของเฟืองต่อไป

คำสำคัญ: เฟืองเฉียง, การแตกหัก, ความล้า, รถยนต์บรรทุกขนาดเล็ก

ABSTRACT

The fracture of a driving helical gear of 5th position gearing system in the gear-box of some pick-up car which was approximately used as 6 years of service. This gear helical was already made from low alloy steel as JIS-SCr 420. It has been determined in many ways on the failure analysis of this helical gear i.e. 1) Composition (wt%) analysis with a spectrometer, 2) Vickers test, 3) Microstructural analysis with optical microscope, which the crack of surface layer and energy dispersive spectroscopy using a scanning electron microscope, 4) Helical gear's AGMA bending stress equation analysis and 5) All results comparison with finite element method. This analysis of summary results of this driving helical gear was determined by the fatigue, which the load of bending stress was over taken than tensile strength of the material (1,300 MPa). The fracture characteristic of the helical gear's surface was expected with the fracture as transgranular and Intergranular, which had been absolutely observed as the brittle fracture. On the axial of helical gear was fractured as the cleavage features and pitting. This mixing failure area can be illustrated by the brittle and ductile fracture. It can be seen that the mixing failure area of oxide inclusion with carbide surrounding before the liquid state of material will be solidified which as the failure cause of this driving helical gear. The analysis of summary results can be accorded with the assumption of this research and which as the information for a protection of any failure gearing.

KEYWORDS: helical gear, failure, fatigue, Pick-up car

1. บทนำ

งานวิจัยนี้มุ่งศึกษาความเสียหายของเฟืองเฉียงที่เกิดขึ้นในตำแหน่งเกียร์ 5 ของรถปิ๊คอัพที่มีกำลังขับ 120 kW ผ่านการใช้งานมา 6 ปี เฟืองทำจากเหล็กกล้าผสมต่ำตามมาตรฐานของ JIS-SCr 420 ที่ได้รับการออกแบบและผ่านกระบวนการผลิต การอบชุบผิวแข็งที่เหมาะสม โดยส่วนใหญ่ความเสียหายที่เกิดกับเฟืองเฉียงนั้นเกิดจากความเค้นดัดในฟันเฟือง (Bending Stress) และความเค้นที่ผิวสัมผัสของฟันเฟือง (Contact Stress) ความเสียหายของฟันเฟืองจากสาเหตุที่กล่าวมานั้น เกิดจากความล้า (Fatigue) เพราะแรงที่กระทำกับฟันเฟืองเป็นแบบกระทำซ้ำกันและมีความถี่ตามรอบการทำงานของเฟือง การวิเคราะห์ความเสียหายของเฟืองสามารถหาได้หลายวิธี เช่น การตรวจสอบด้วยภาพถ่าย การตรวจสอบความแข็งของเฟืองด้วยวิธีวิกเกอร์ส การตรวจสอบด้วยกล้องจุลทรรศน์แบบใช้แสง (OM) และกล้องจุลทรรศน์อิเล็กตรอนแบบส่องกราด (SEM) การตรวจสอบเปอร์เซ็นต์ธาตุผสมด้วยเครื่อง Spectrometer และวิธี EDS (Energy Dispersive spectroscopy) ความเค้นดัดของเฟืองเฉียงสามารถวิเคราะห์ได้โดยใช้สมการของลูอิสตามมาตรฐานของ AGMA ซึ่งวิธีนี้มีความยุ่งยากมากพอสมควร ปัจจุบันการวิเคราะห์ความเค้นรูปแบบหนึ่งที่ได้รับความนิยมอย่างกว้างขวางคือ วิธีไฟไนต์เอลิเมนต์ เครื่องมือต่าง ๆ ที่กล่าวมาล้วนแต่เป็นเครื่องมือที่มีการใช้งานกันอย่างแพร่หลายในอุตสาหกรรมรถยนต์

2. วิธีการทดลอง

วิธีการดำเนินงานวิจัยสามารถจำแนกได้หลายลักษณะ ดังนี้

2.1 การตรวจสอบด้วยภาพถ่าย

การตรวจสอบด้วยภาพถ่ายของเฟืองที่เสียหายจะเห็นว่าจำนวนของฟันเฟืองที่แตกอยู่ติด ๆ กันมีสาเหตุเกิดจากความล้าตัวของวัสดุดังรูปที่ 1 จะเห็นได้ว่าการแตกมีลักษณะเป็นสามเหลี่ยมขนาดใหญ่ที่ปลายด้านหนึ่งของฟันเฟืองและมีพื้นที่เป็น 1/3 ของความกว้างฟันเฟือง [1]

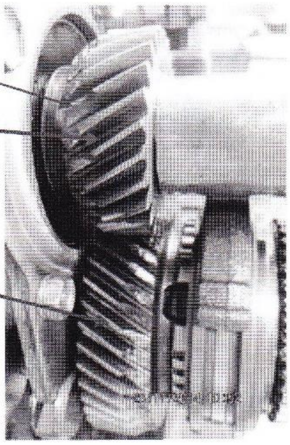

รูปที่ 1 การแตกหักของเฟืองเฉียงที่ตำแหน่งเกียร์ 5

พิจารณารูปที่ 2 ภาพขยายพื้นผิวรอยแตกหักของฟันเฟืองแสดงให้เห็นจุดเริ่มต้นของรอยแตกมีลักษณะเป็นแบบ Beach marks คือการแตกมีลักษณะแบนราบต่อเนื่องไปจนถึงส่วนปลายของรอยแตกจุดเริ่มต้นของรอยแตกจะมองเห็นได้อย่างชัดเจนดังรูปที่ 2 ที่มาของรอยแตกเกิดขึ้นในแนวพิตช์ (Pitch line) ใกล้กับปลายด้านหนึ่งของฟันเฟืองซึ่งบอกได้ว่าโหลดที่กระทำสูงสุดอยู่ที่จุดนี้ [1]

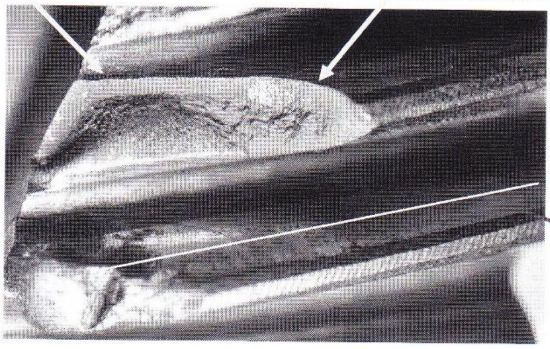

รูปที่ 2 ขยายพื้นผิวรอยแตกหักของฟันเฟืองเฉียง

2.2 การทดสอบความแข็ง

การทดสอบความแข็งของเฟืองเฉียงด้วยการวัดความแข็งแบบวิกเกอร์สด้วยเครื่องมือวัดของ (Mitutoyo model MVKH1) การวัดความแข็งตามแนวภาคตัดขวาง ผลที่ได้ดังรูปที่ 3 ค่าความแข็งสูงสุดที่ผิวของเฟืองเท่ากับ 780 HV (63.3 HRC) และค่าความแข็งต่ำสุดที่บริเวณใจกลางของเฟืองเท่ากับ 310 HV (31 HRC)

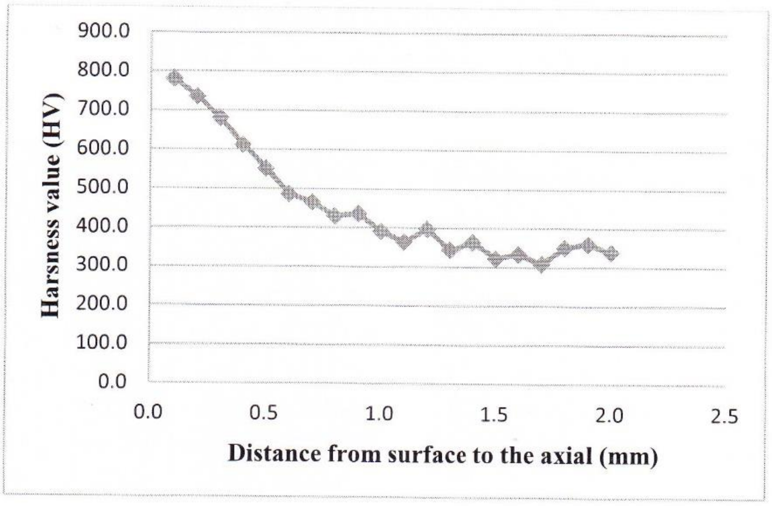

รูปที่ 3 ค่าความแข็งเฟืองที่เสียหายโดยวัดจากขอบผิวด้านนอกไปถึงแกนกลางของเฟือง

2.3 การตรวจสอบผลทางเคมี

การตรวจสอบสมบัติทางเคมีของเฟืองโดยใช้เครื่อง Spectrometer รุ่น ARL 3640 ผลที่ได้ออกมาเป็นเปอร์เซ็นต์ส่วนประกอบทางเคมีดังแสดงในตารางที่ 1 เฟืองเกียร์ทำจากเหล็กกล้าผสมต่ำตามมาตรฐาน JIS-SCr 420 ที่มีโครเมียมเป็นส่วนผสมสำคัญ [2]

ตารางที่ 1 การเปรียบเทียบส่วนผสมทางเคมีของเฟืองกับมาตรฐานของ JIS-SCr 420

วัสดุ	C	Si	Mn	P	S	Ni	Cr
เฟืองที่เสียหาย ผิวเฟือง	0.564	0.246	0.856	0.019	0.013	0.019	1.021
แกนกลาง	0.223	0.250	0.835	0.020	0.017	0.026	1.116
เฟืองมาตรฐาน Scr 420	0.18-0.23	0.15-0.35	0.60-0.90	$\leq$ 0.030	$\leq$ 0.030	$\leq$ 0.250	0.90-1.20

2.4 การตรวจสอบโครงสร้างจุลภาค

การตรวจสอบโครงสร้างจุลภาคของเฟืองที่เสียหายโดยใช้กล้องจุลทรรศน์รุ่น OLYMPUS LASER MICROSCOPES: OLS 4000 ที่ผิวของเฟืองมีส่วนประกอบของมาร์เทนไซต์ซึ่งผ่านการเทมเปอร์ดังรูปที่ 4a ส่วนที่บริเวณใจกลางของเฟืองจะมีส่วนประกอบของโครงสร้างจุลภาคที่เป็นเฟอร์ไรต์ผสมเพิร์ลไลต์ดังรูปที่ 4b จากการสังเกตโครงสร้างจุลภาคและผลจากค่าความแข็งสามารถบอกได้ว่าเฟืองชิ้นนี้ได้รับการเพิ่มความแข็งด้วยการชุบแข็งที่ผิวโดยวิธีคาร์เบอไรซิง (Carburizing) จนทำให้ผิวรอบนอกมีส่วนประกอบของมาร์เทนไซต์ (Full martensite) ส่วนชั้นด้านในจะเป็นเฟอร์ไรต์ผสมเพิร์ลไลต์เต็มรูปแบบที่ไม่พบความผิดปกติในโครงสร้างจุลภาคของเฟือง [3]

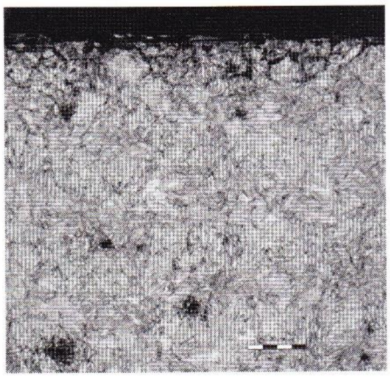

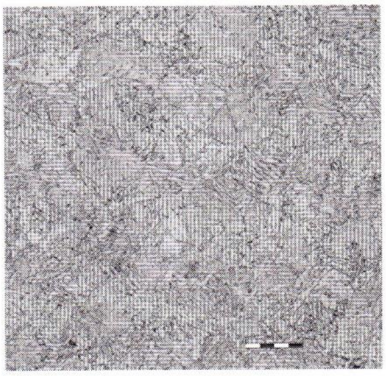

รูปที่ 4 โครงสร้างจุลภาคของเฟืองที่กำลังขยาย 2129X (a) รูปที่ผิวของเฟืองมีส่วนประกอบของมาร์เทนไซต์ (b) รูปที่แกนกลางของเฟืองจะมีส่วนประกอบของเฟอร์ไรต์และเพิร์ลไลต์

การตรวจสอบรอยแตกหักของฟันเฟืองเกียร์โดยใช้กล้องจุลทรรศน์อิเล็กตรอนไมโครสโคปแบบส่องกราด หรือ Scanning Electron Microscope: SEM (HITACHI: S-3400N) ดังรูปที่ 5 ถ่ายบริเวณผิวรอบนอกของเฟืองแสดงให้เห็นว่ามีการแตกผ่านเกรน (Transgranular) ซึ่งเป็นผลของการเปลี่ยนแนวระนาบที่แยก (Cleavage features) ออกจากเกรนหนึ่งไปสู่อีกเกรนหนึ่งและมองเห็นการแตกระหว่างเกรน (Intergranular fracture) รอยแตกจะเกิดตามแนวขอบเกรนซึ่งโดยปกติเกิดจากขอบเกรนซึ่งอ่อนแอและเปราะ ลักษณะดังกล่าวเป็นการแตกหักแบบเปราะ รูปที่ 6 ถ่ายในบริเวณแกนกลางของเฟืองแสดงให้เห็นว่ามีลักษณะการแตกแบบแยกออก อีกทั้งมีลักษณะเป็นหลุม (Pit) อีกด้วย ความเสียหายในบริเวณนี้เป็นแบบผสมซึ่งมีการแตกหักแบบเปราะและแบบเหนียวปนกัน [4]

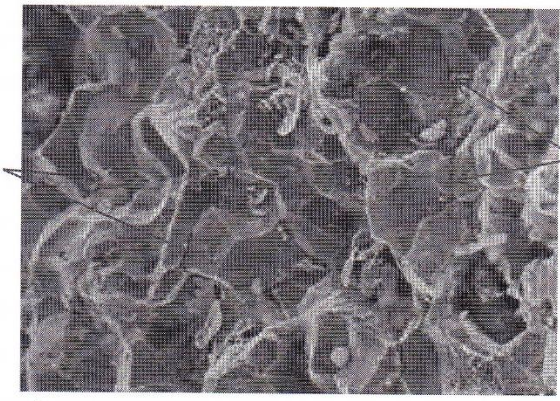

รูปที่ 5 ภาพจากกล้องขยายกำลังสูง (SEM) ถ่ายบริเวณผิวรอบนอกของเฟืองสามารถมองเห็นการแตกผ่านเกรนและการแตกหักระหว่างเกรน กำลังขยาย 500x (10 μm)

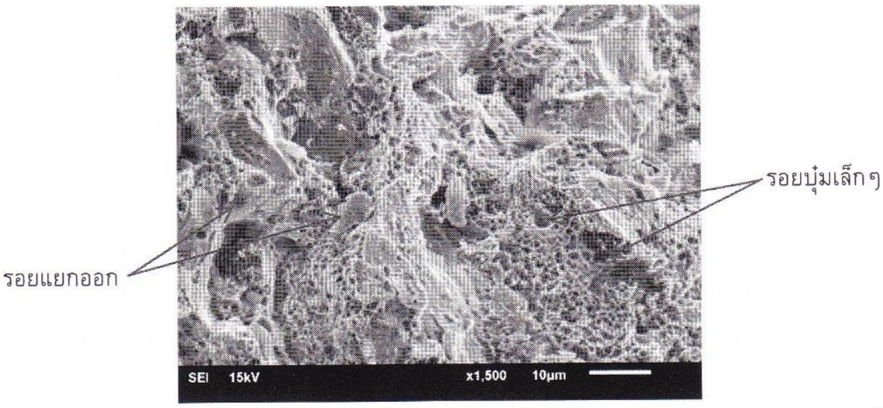

รูปที่ 6 ภาพจากกล้องขยายกำลังสูง (SEM) ถ่ายที่ใจกลางของเฟืองสามารถมองเห็นลักษณะการแตกแบบแยกออกและมีลักษณะเป็นรอยบุ๋มเล็ก ๆ โดยมีกำลังขยาย 1500x (10 μm)

การวิเคราะห์ธาตุเชิงปริมาณด้วย EDS (Energy Dispersive Spectroscopy) พิจารณาจุดที่เกิดการรวมตัวกันของธาตุ (Included Elements) ดังแสดงในรูปที่ 7 แนวของการสแกนจะเห็นว่ามีธาตุโครเมี่ยมสูงที่สุดในบริเวณรอบวงกลมสีขาว หากพิจารณารูปที่ 8 ตรงแนวกราฟ EDS จะเห็นว่ามีธาตุโครเมี่ยมที่เพิ่มสูงขึ้น ส่วนองค์ประกอบอื่นๆ คือเหล็ก คาร์บอน แมงกานีส ซิลิกอน และออกไซด์ มีการรวมตัวกันเป็นส่วนผสมของออกไซด์ล้อมรอบด้วยคาร์ไบด์ก่อนที่จะมีการเปลี่ยนสถานะจากของเหลวกลายเป็นของแข็ง สรุปผลได้ว่าการแข็งตัวเป็นเหล็กกล้าผสมต่ำจะมีองค์ประกอบของออกไซด์ (สีเข้ม) ล้อมรอบด้วยคาร์ไบด์ Fe_3C [5]

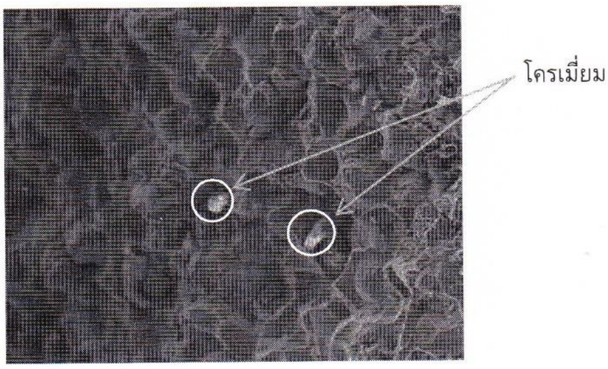

รูปที่ 7 จุดที่เกิดการรวมตัวกันของธาตุต่าง ๆ ซึ่งมีโครเมี่ยมสูงสุด กำลังขยาย 200x (20 μm)

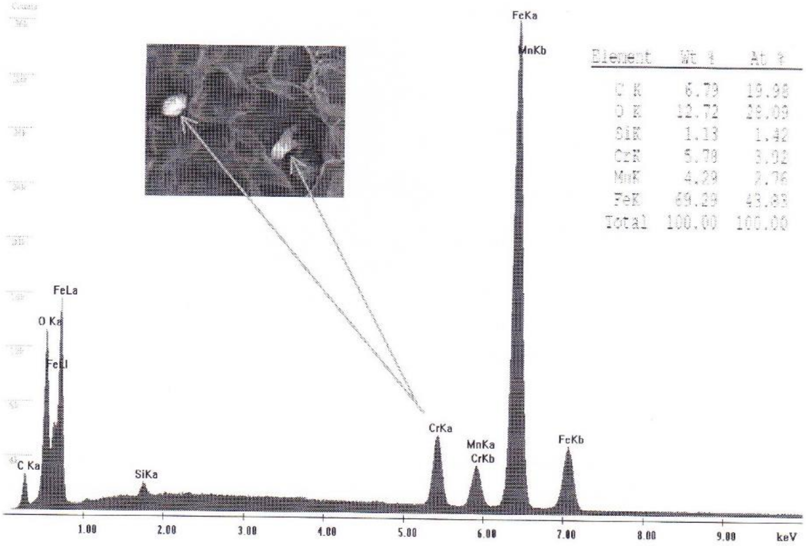

รูปที่ 8 กราฟ EDS จุดที่เกิดการรวมตัวกันของธาตุผสมต่ำ

2.5 การวิเคราะห์ความเค้นดัดโดยสมการของลูอิสเปรียบเทียบกับวิธีไฟไนต์อิลิเมนต์

ส่วนประกอบต่าง ๆ ของเฟืองเฉียงแสดงในตารางที่ 2

ตารางที่ 2 ขนาดพร้อมส่วนประกอบของเฟืองเฉียง

ลักษณะ	สัญลักษณ์	ขนาด	หน่วย
กำลังสูงสุดที่ความเร็วรอบ/นาที	H @ n_p	120 @ 3200	kW @ rpm
จำนวนฟันเฟืองตาม	N_p	26	ฟัน
จำนวนฟันเฟืองขับ	N_G	46	ฟัน
เส้นผ่านศูนย์กลางเฟืองตาม	d_p	64	มม
เส้นผ่านศูนย์กลางเฟืองขับ	d_G	109	มม
โมดุล	m	2.25	-
มุมกด	ϕ	20°	องศา
มุมฮีลิก	ψ	30°	องศา
ความกว้างของฟันเฟือง	F	23	มม

สมการความเค้นดัดของลูอิสตามมาตรฐานของ AGMA [6]

$$\sigma_b = \frac{W_t K_o K_m}{K_v F m J} \tag{1}$$

ขนาดเส้นผ่านศูนย์กลางพิตช์ของเฟืองตาม (d_p) = mN_P = 2.25 x 26 = 58.5 mm

ความเร็วแนวพิตช์ (V) = $\frac{\pi d_p n_p}{60\times 10^3}$ = $\frac{\pi\times 58.5\times 3200}{60\times 1000}$ = 9.80 m/s

แรงส่งกำลังของเฟือง (W_t) = $\frac{H}{V}$ = $\frac{120}{9.80}$ = 12.24 kN

แฟคเตอร์โหลดเกินกำลัง (K_o) = 1.25

แฟคเตอร์การกระจายของโหลด (K_m) = 1.3

ไดนามิคแฟคเตอร์ (K_v) = $\frac{3.5}{3.5+\sqrt{V}}$ = $\frac{3.5}{3.5+\sqrt{9.80}}$ = 0.53

แฟคเตอร์เรขาคณิต (J) = 0.26

$$\sigma_b = \frac{12.24\times 10^3\times 1.25\times 1.3}{0.53\times 23\times 2.25\times 0.26} = 2{,}789.17 \text{ N/mm}^2$$

วิเคราะห์ความเค้นดัดด้วยวิธีไฟไนต์อิลิเมนต์

ผลของการวิเคราะห์ความเค้นดัดโดยใช้โปรแกรม Solid works 14 ตามเงื่อนไขขอบเขตที่ถูกนำมาใช้ในฟันเฟืองเกียร์แสดงให้เห็นว่าความเค้นที่กระทำกับฟันเฟืองเกิดขึ้นดังรูปที่ 9 และค่าความเค้นดัดทีเกิดขึ้นกับฟันเฟืองจะมีการเปลี่ยนแปลงตามแรงที่ส่งกำลังของเฟือง W_t ที่เพิ่มขึ้นดังแสดงในตารางที่ 3 [7]

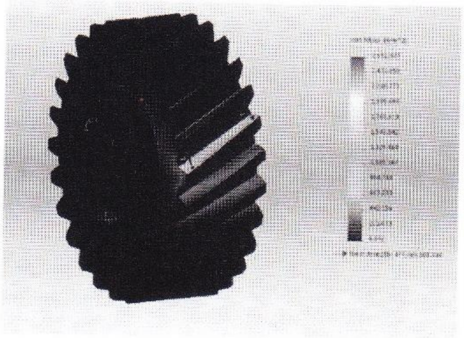

รูปที่ 9 ค่าความเค้นดัดที่เกิดจากแรงส่งกำลังของเฟือง W_t = 12.24 kN

ตารางที่ 3 เปรียบเทียบค่าความเค้นดัดระหว่างสมการของลูอิสกับผลทางไฟไนต์เอลิเมนต์

แรงบิด (N.m)	แรงส่งกำลังของเฟือง (kN)	ค่าความเค้นดัด σ_b (MPa)	Von Mises (Solid 14) (MPa)
96	2.97	629.29	644.76
175	5.44	1173.22	1175.35
243	7.54	1655.68	1632.05
301	9.32	2084.45	2021.60
351	10.89	2435.59	2357.41
395	12.24	2789.17	2,652.92
434	13.45	3077.39	2914.86
468	14.51	3388.75	3143.25

จากรูปที่ 10 ค่าความเค้นดัดที่ได้จากการคำนวณและวิธีไฟไนต์เอลิเมนต์มีค่าที่ใกล้เคียงกันมาก ความเค้นดัดจะเพิ่มขึ้นตามแรงบิดที่เพิ่มขึ้น สรุปคือในกรณีที่แรงบิดมีมากเกินกว่า Tensile strength 1300 N/mm^2 [8] จึงเป็นสาเหตุหนึ่งที่ทำให้เฟืองแตกในระหว่างเปลี่ยนเกียร์

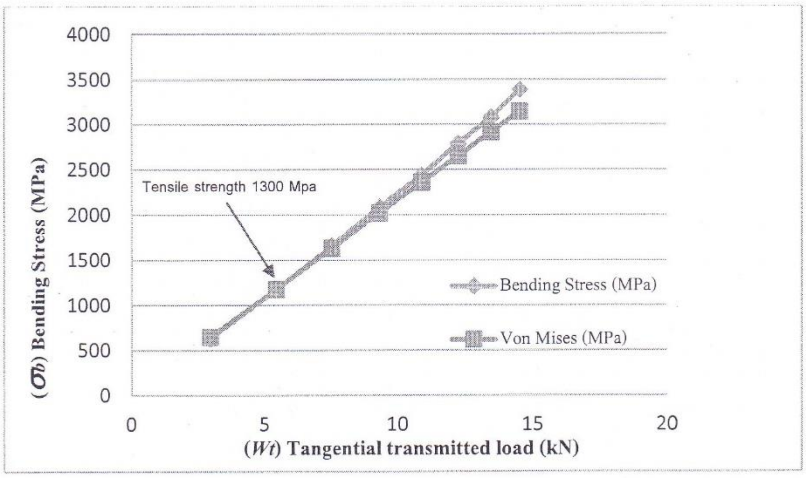

รูปที่ 10 เปรียบเทียบค่าความเค้นดัดระหว่างสมการของ AGMA กับวิธีไฟไนต์อิลิเมนต์

3. ผลการทดลองและอภิปราย

การตรวจสอบความเสียหายด้วยภาพถ่ายแสดงให้เห็นรอยแตกหักเป็นสามเหลี่ยมที่ปลายของฟันเฟืองทั้งนี้พื้นที่รอยแตกเป็นหนึ่งในสามของความกว้างฟันเฟืองซึ่งเกิดจากความล้าของวัสดุ ซึ่งบอกได้ว่ามีโหลดกระทำสูงสุดเกิดขึ้นในแนวพิตช์ของฟันเฟือง

จากการทดสอบความแข็งพบว่าค่าความแข็งสูงสุดอยู่ที่ผิวของเฟืองมีค่าเป็น 63.3 HRC และค่าความแข็งต่ำสุดที่บริเวณใจกลางของเฟือง 31 HRC การวิเคราะห์โครงสร้างจุลภาคด้วย OM จะเห็นว่าที่ผิวรอบนอกมีส่วนประกอบของมาร์เทนไซต์ ส่วนบริเวณใจกลางมีส่วนประกอบของเฟอร์ไรต์กับเพิร์ลไลต์ ผลจากค่าความแข็งและโครงสร้างจุลภาคสามารถบอกได้ว่าเฟืองชิ้นนี้ ได้รับการเพิ่มความแข็งด้วยการชุบแข็งที่ผิวโดยวิธีคาร์เบอร์ไรซิง (Carburizing) และไม่พบความผิดปกติในโครงสร้างจุลภาคของเฟือง

การตรวจสอบรอยแตกของเฟืองด้วย SEM พบว่าลักษณะของรอยแตกบริเวณผิวรอบนอกของเฟืองมีการแตกผ่านเกรนและการแตกระหว่างเกรน ซึ่งเป็นการแตกหักแบบเปราะ ส่วนที่แกนกลางของเฟืองมีการแตกแบบแยกออกและแบบรอยบุ๋ม ความเสียหายในบริเวณนี้เป็นแบบผสมคือมีการแตกหักแบบเปราะและแบบเหนียวปนกัน

การวิเคราะห์เปอร์เซ็นต์ธาตุผสมด้วยวิธี EDS จุดที่เกิดการรวมตัวกันของธาตุผสมจะเห็นว่ามีธาตุโครเมี่ยมที่เพิ่มสูงขึ้น ส่วนองค์ประกอบอื่นคือเหล็ก คาร์บอน แมงกานีส ซิลิกอน และออกไซด์ ผลที่ได้แสดงให้เห็นว่ามีการรวมตัวกันเป็นส่วนผสมของออกไซด์ล้อมรอบด้วยคาร์ไบด์ก่อนที่จะมี

การเปลี่ยนสถานะจากของเหลวเป็นของแข็ง สรุปคือเปอร์เซ็นต์การรวมตัวของออกไซด์กับคาร์ไบด์ในโครงสร้างจุลภาคจะเป็นสาเหตุของความเสียหายที่เกิดขึ้นในฟันเฟือง

ผลการคำนวณที่ได้จากสมการของลูอิสตามมาตรฐานของ AGMA เปรียบเทียบกับวิธีไฟไนเอลิเมนต์นั้นมีค่าความเค้นดัดมีค่าใกล้เคียงกันมากเมื่อแรงบิดเพิ่มสูงขึ้นจนเกินค่า Tensile strength ก็เป็นอีกสาเหตุหนึ่งที่ทำให้เฟืองเกิดการแตกหัก

4. สรุปผลการวิจัย

งานวิจัยนี้เป็นการวิเคราะห์ความเสียหายของเฟืองเฉียงที่ใช้ในรถปิ๊กอัพ โดยมีการวิเคราะห์สมบัติทางเคมี สมบัติทางกล และโครงสร้างจุลภาคของเฟืองที่ทำมาจากเหล็กกล้าผสมต่ำ JIS-SCr 420 ซึ่งผ่านกระบวนการผลิตและการชุบผิวแข็งที่เหมาะสม จากการวิเคราะห์ดังกล่าวสามารถสรุปผลได้ดังนี้

1. ผิวรอบนอกของเฟืองมีการแตกผ่านเกรนและการแตกระหว่างเกรน ลักษณะดังกล่าวเป็นการแตกหักแบบเปราะ โครงสร้างจุลภาคมีส่วนประกอบของมาร์เทนไซด์ ในบริเวณแกนกลางของเฟืองมีการแตกแบบแยกออกและมีลักษณะเป็นรอยบุ๋ม ความเสียหายเป็นแบบผสมซึ่งมีการแตกหักแบบเปราะและแบบเหนียวปนกัน โครงสร้างจุลภาคมีส่วนประกอบของเฟอร์ไรต์ผสมกับเพิร์ลไลต์

2. รอยแตกหักเกิดจากความล้าแล้วการเพิ่มระดับแรงกระทำในบริเวณใจกลางจะเกิดอย่างช้าๆ ในระหว่างที่ระดับความเค้นเพิ่มขึ้นทีละน้อยนี้รอยแตกจากความล้าก็ขยายตัวต่อไปจนกระทั่งถึงความล้าวิกฤต ทำให้เฟืองไม่สามารถรับแรงกระทำต่อไปได้อีกจึงเป็นสาเหตุที่ทำให้เฟืองเกิดการแตกหัก

3. เปอร์เซ็นต์การรวมตัวของออกไซด์กับคาร์ไบด์ในโครงสร้างจุลภาคที่ไม่เหมาะสม (Inclusion) เป็นสาเหตุของความเสียหายที่เกิดขึ้นในฟันเฟือง เช่นกรณีนี้โครงสร้างจุลภาคของออกไซด์ซึ่งล้อมรอบด้วยคาร์ไบด์ที่เกิดขึ้นก่อนที่จะมีการเปลี่ยนสถานะ ซึ่งเป็นสิ่งที่ยากต่อการควบคุมในการผลิต โดยส่วนใหญ่จะทำด้วยการเติมสารที่ช่วยขับออกไซด์

4. ความเค้นดัดที่เกิดจากแรงบิดมีค่ามากกว่า Tensile strength ของวัสดุเฟืองดังผลที่ได้จากวิธีการคำนวณและวิธีไฟไนต์เอลิเมนต์ เป็นตัวบ่งบอกได้ว่าค่าความเค้นดัดสูงสุดไม่ควรเกิน 1300 N/mm2 ซึ่งจะเป็นประโยชน์ต่อผู้ออกแบบเฟือง (จากกรณีดังกล่าวก็จะช่วยให้ผู้ที่นำรถยนต์ไปเพิ่มกำลังจะได้ตระหนักถึงผลเสียหายที่ตามมาจากการเพิ่มความแรงของเครื่องยนต์ เพราะจะมีผลกับเกียร์และระบบส่งกำลัง)

กิตติกรรมประกาศ

ผู้วิจัยขอขอบคุณอาจารย์ที่ปรึกษารองศาสตราจารย์ ดร.กัณวริช พลูปราชญ์ ศาสตราจารย์ ดร.ฮาดี ชูดันโต นอกจากนี้ขอขอบคุณ ผู้ช่วยศาสตราจารย์ ดร.วิรัตน์ จอมขวา ผู้ช่วยศาสตราจารย์ ชานนท์ มูลวรรณ และ คุณสำเริง เนตรภู่ ที่ได้ให้ข้อเสนอแนะในการทำงานวิจัย สิ่งที่ลืมมิได้คือ ความอนุเคราะห์ต่อการใช้เครื่องมือวิเคราะห์จากศูนย์เทคโนโลยีโลหะและวัสดุแห่งชาติ

References

[1] Osman Asi. (2005). "Fatigue Failure of a Helical Gear in a Gearbox". **Engineering Failure Analysis.** Vol.13. (7): 1116-1125.

[2] JIS G 4053. (2003). **Japanese Industrial Standard**. First English Edition. Japan.

[3] Samroeng Netpu and Panya Srichandr. (2012). "Failure Analysis of a Helical Gear in a Gearbox Used in a Steel Rolling Mill". **Journal of Materials Science and Engineering.** : 289-294.

[4] William D. Callister, Jr. (2005). **Materials Science and Engineering an Introduction**. Bangkok: Top Publishing Co., Ltd. (In Thai)

[5] Samroeng Netpu and Panya Srichandr. (2013). "Failure Analysis of a Helical Gear in a Power Plant". **Engineering Failure Analysis**. Vol. 32: 81-90.

[6] Chamroon Tantipisalkul. (2007). **Mechanical Engineering Design 1**. 4th edition. Bangkok: Threelada Ltd. (In Thai)

[7] J. Venkatesh and Mr. P. B. G. S. N. Murthy. (2014). "Design and Structural Analysis of High Speed Helical Gear Using Ansys". **J. Venkatesh Int. Journal of Engineering Research and Applications.** Vol. 4. Issue 3: 1-5.

[8] Saarstahl. **Material Specification Sheet.** Available: http://www.saarstahl.com/fileadmin/saarstahl_extranet/images/04_produkte/walzstahahlsorten/English/7147_7149_20MnCr5_20MnCrS5.pdf.

ประวัติผู้เขียนบทความ

วิษณุ บุญมาก ตำแหน่งอาจารย์ สาขาเทคโนโลยีรถยนต์ วิทยาลัยเทคโนโลยียานยนต์โตโยต้า หมายเลขโทรศัพท์ 086-9908096 อีเมล์: boonmagvisa@gmail.com

กัณวริช พลูปราชญ์ ตำแหน่งรองศาสตราจารย์ ดร. ประจำภาควิชาวิศวกรรมเครื่องกล คณะวิศวกรรมศาสตร์ มหาวิทยาลัยศรีนครินทรวิโรฒ หมายเลขโทรศัพท์ 089-1411135 อีเมล์: pganwarich@yahoo.com

VITAE

VITAE

Name:	Mr. Visanu Boonmag
Date of Birth:	1 December 1969
Place of Birth:	Chiangmai, Thailand
Address:	485/3 Moo 4 Soi Phaholyothin 52, Klongtanon, Saimai district, Bangkok 10220, Thailand

Education Background:

1986	Vocational Education in Industrial Technology (Automotive Mechanical) Polytechnic Lanna School
1989	Diploma of Vocational Education in Industrial Technology (Automotive Mechanical) Udonthani Technical College
1996	Bachelor of Industrial Technology (Mechanical Engineering) Saint John’s University
2008	Bachelor of Engineer (Mechanical Engineering) Phatumwan Institute of Technological
2016	Master of Engineering (Mechanical Engineering) Srinakharinwirot University